



Universiteit
Leiden
The Netherlands

Squaramide-based supramolecular polymers : from self-assembly to in vivo application

Saez Talens, V.

Citation

Saez Talens, V. (2018, December 10). *Squaramide-based supramolecular polymers : from self-assembly to in vivo application*. Retrieved from <https://hdl.handle.net/1887/67527>

Version: Not Applicable (or Unknown)

License: [Licence agreement concerning inclusion of doctoral thesis in the Institutional Repository of the University of Leiden](#)

Downloaded from: <https://hdl.handle.net/1887/67527>

Note: To cite this publication please use the final published version (if applicable).

Cover Page



Universiteit Leiden



The handle <http://hdl.handle.net/1887/67527> holds various files of this Leiden University dissertation.

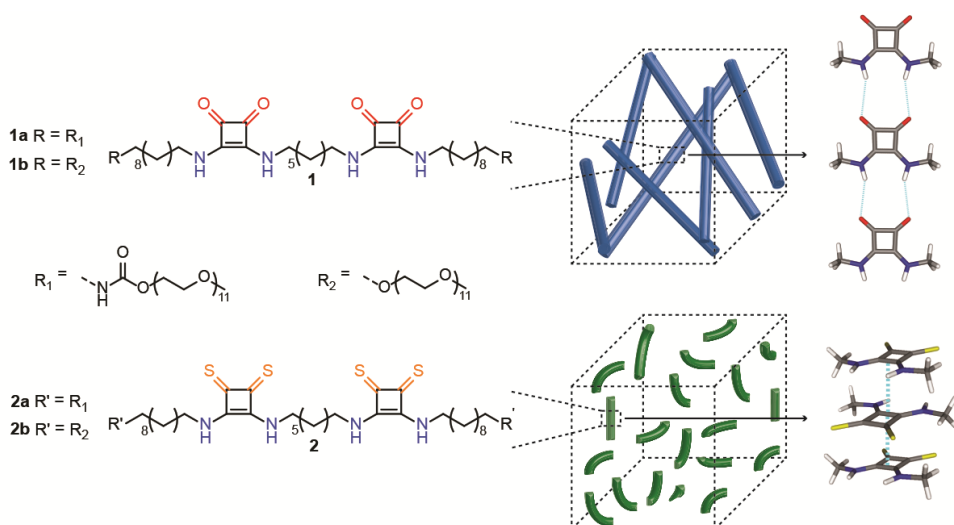
Author: Saez, Talens V.

Title: Squaramide-based supramolecular polymers : from self-assembly to in vivo application

Issue Date: 2018-12-10

CHAPTER 3

A self-assembly mode “Tug-of-war” in squaramide-based supramolecular polymers driven by aromaticity-modulated hydrogen bonding



This chapter was prepared as an original research paper: Victorio Saez Talens, Mahsa Boraghi, Raisa Rudge, Chia-Hua Wu, Thuat T. Trinh, Pablo Englebienne, Ilja K. Voets, Judy I. Wu, Roxanne E. Kieltyka

3.1 Abstract

Despite a growing understanding of the factors driving monomer self-assembly to form supramolecular polymers, the effect of aromaticity gain in hydrogen-bonding cyclic π -conjugated synthons is overlooked. Herein, I demonstrate the interplay of aromaticity gain and hydrogen bonding on “switching” the self-assembly modes of squaramide-based bolaamphiphiles. Surprisingly, O \rightarrow S substitution in squaramide synthons resulted in supramolecular polymers with increased fiber flexibility and lower degrees of polymerization. Computation and experimental studies suggest that both oxo- and thiosquaramide bolaamphiphiles self-assemble through hydrogen-bonding interactions, but into drastically different arrangements: “head-to-tail” versus “stacked”, respectively. Computed energetic and magnetic criteria of aromaticity reveal that both modes of self-assembly increase the aromatic character of the squaramide synthons, giving rise to stronger intermolecular hydrogen bonding interactions in the resultant supramolecular polymer structures. These examples illustrate the effects of aromaticity gain in cyclic π -conjugated synthons on supramolecular polymerization, and suggest that aromaticity-modulated hydrogen bonding (AMHB) should be considered in monomer design.

3.2 Introduction

Supramolecular polymers have a dynamic character that endows them with unique properties, such as responsiveness and self-healing,¹⁻⁴ leading to numerous potential applications in biomedical materials, adhesives, inks or personal care products.⁵⁻⁷ To gain access to such materials, the monomers are engineered to engage in various non-covalent interactions including hydrogen-bonding,⁸⁻¹⁰ aromatic interactions, solvophobicity and van der Waals, that drive their self-assembly into hierarchical architectures through stacking or molecular recognition of polymeric precursors.¹¹⁻²⁰ The growing number of synthesized monomers has contributed significantly to the development of general design rules to facilitate monomer self-assembly in organic solvents and water. However, to further guide their rational design, it is necessary to understand factors that influence the strength of noncovalent interactions either within or between monomers. Here, I demonstrate the impact of the combination of hydrogen bonding and aromaticity gain on the mode of monomer self-assembly in a supramolecular polymer.

Aromaticity, with its near 150-year old history starting with Kekulé, continues to fascinate chemists with its peculiar energetic, geometric, and spectroscopic manifestations in molecules. Nevertheless, Wu, Jackson and co-workers demonstrated computationally²¹⁻²³ and experimentally²⁴ that aromaticity can also significantly influence the strengths of *intermolecular* hydrogen bonding interactions beyond the traditional electrostatic-based view of hydrogen bonding through a reciprocal aromaticity-modulated hydrogen bonding (AMHB) relationship. These authors demonstrated that hydrogen bonding interactions that increase cyclic $4n + 2$ π -electron delocalization (i.e., increase aromaticity) in heterocycles can be strengthened, while those that decrease cyclic $4n + 2$ π -electron delocalization (decreased aromaticity) are weakened.^{21,22,24} Such effects are especially pronounced when hydrogen-bonded assemblies of cyclic π -conjugated motifs are considered, as the effects of aromaticity gain in each of the synthon rings can add up to an astonishing overall aromatization of the self-assembled system.²³ Concurrently, the Kielyka group reported the self-assembly of a novel squaramide-based bolaamphiphile that takes

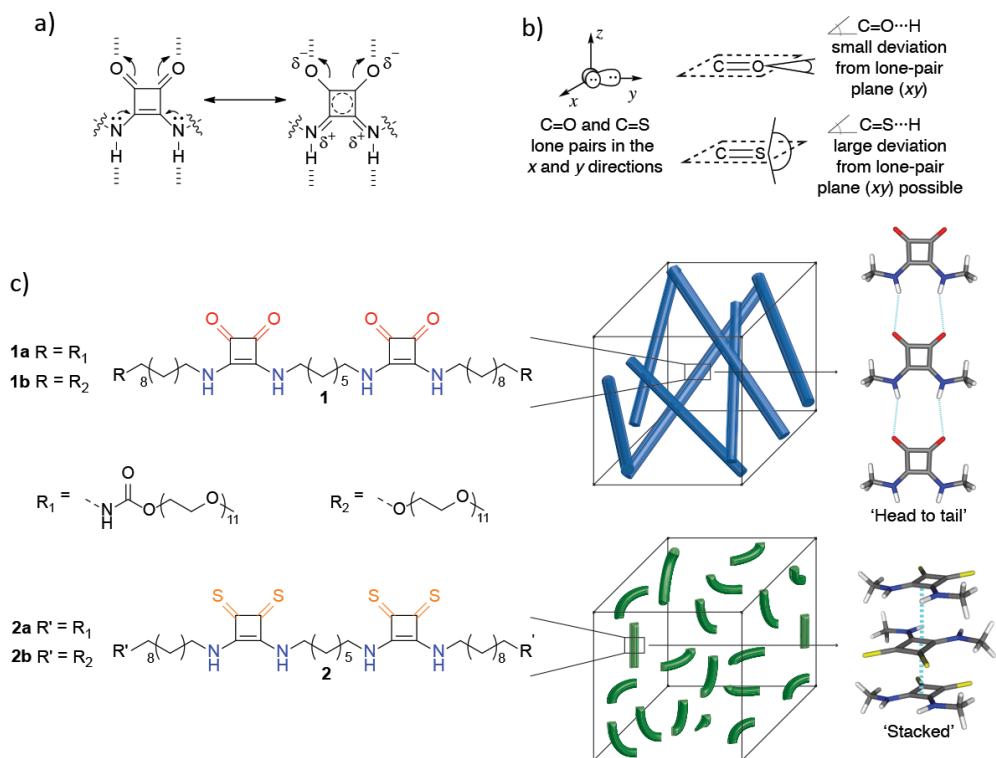


Figure 3.1. (a) Aromaticity-modulated hydrogen bonding (AMHB) in oxosquaramide; the resonance form on the right shows increased cyclic 2π -electron delocalization in the four membered ring. (b) Carbonyls ($\text{C}=\text{O}$) typically form hydrogen bonds with small deviations from the lone-pair (xy) plane, but thiocarbonyls ($\text{C}=\text{S}$) can form hydrogen bonds with $\text{C}=\text{S}\cdots\text{H}$ angles of close to 90° . As a result, $\text{C}=\text{O}$ and $\text{C}=\text{S}$ containing synthons are expected to promote drastically different self-assembly modes. (c) Structures of the oxosquaramide (**1a** and **1b**) and thiosquaramide (**2a** and **2b**) bolaamphiphiles under study. **1a** and **1b** self-assemble into rigid fibers (*top*), while **2a** and **2b** self-assemble into short flexible rod-like structures (*bottom*). This disparity is attributed to the “head-to-tail” self-assembly of the oxosquaramides versus “stacked” self-assembly of the thiosquaramides.

advantage of aromaticity gain to form robust supramolecular polymers in water.²⁵ Squaramides²⁶⁻³⁰ are ditopic hydrogen-bonding synthons that can self-associate through two hydrogen bond acceptors ($\text{C}=\text{O}$ groups) and two hydrogen bond donors ($\text{N}-\text{H}$ groups) directly opposite one another on a cyclobutenedione ring. Upon hydrogen bonding at both ends simultaneously, the two $\text{C}=\text{O}$ π -bonds and the two N lone pairs become

polarized to give increased cyclic 2π -electron delocalization ($4n + 2$, $n = 0$) in the four membered ring (Figure 3.1a). Evidence based on experiment and computations revealed that such aromaticity-hydrogen bonding coupling effects intensify with the head-to-tail polymerization of squaramide-based bolaamphiphiles, further reinforcing these interactions.²⁵

Inspired by these results, we performed an O→S exchange of the carbonyl moieties to examine the self-assembly and the aromatic gain on the interaction of thiosquaramide-based bolaamphiphiles relative to the oxosquaramide counterparts. Thiosquaramides, with their demonstrated greater acidity and lipophilicity compared to oxosquaramides,³¹ can potentially self-assemble in very different ways due to the unique supramolecular interactions enabled by the two thiocarbonyls. Thiocarbonyls are typically considered to be weaker hydrogen bond acceptors compared to carbonyls,³² but can engage in effective S⋯ π interactions as well as less directional hydrogen bonding interactions with potentially more than one donor due to the more polarizable nature of the S lone-pairs.^{33,34} Studies based on a survey of carbonyl and thiocarbonyl containing structures in the Cambridge Structural Database (CSD),³⁵ for example, have shown that C=O⋯H interactions generally exhibit small deviations (0 to 20°) from the lone-pair plane (i.e., the plane defined by the two sets of O lone-pairs, see *xy* plane in Figure 3.1b, top), while C=S⋯H interactions can deviate significantly from the lone-pair plane, displaying close to 90° lone-pair plane⋯H angles (Figure 3.1b, bottom). For this reason, C=S-containing synthons may give rise to drastically different modes of self-assembly compared to analogous C=O-containing synthons in the solution phase. Here, we show indeed that, upon O→S exchange, **1** and **2** self-assemble through intermolecular hydrogen-bonding into supramolecular polymers with surprisingly different morphologies: oxosquaramides **1** self-assemble “head-to-tail”, while thiosquaramides **2** “stack” on top of each other as a result of intermolecular hydrogen bonding at a C=S⋯H angle close to 90° (see illustration based on computed results of self-assembled N-methyl-oxosquaramides (**1'**) and N-methyl-thiosquaramides (**2'**) in Figure 3.1c). In this paper, we perform computations and experiments to examine the interplay between

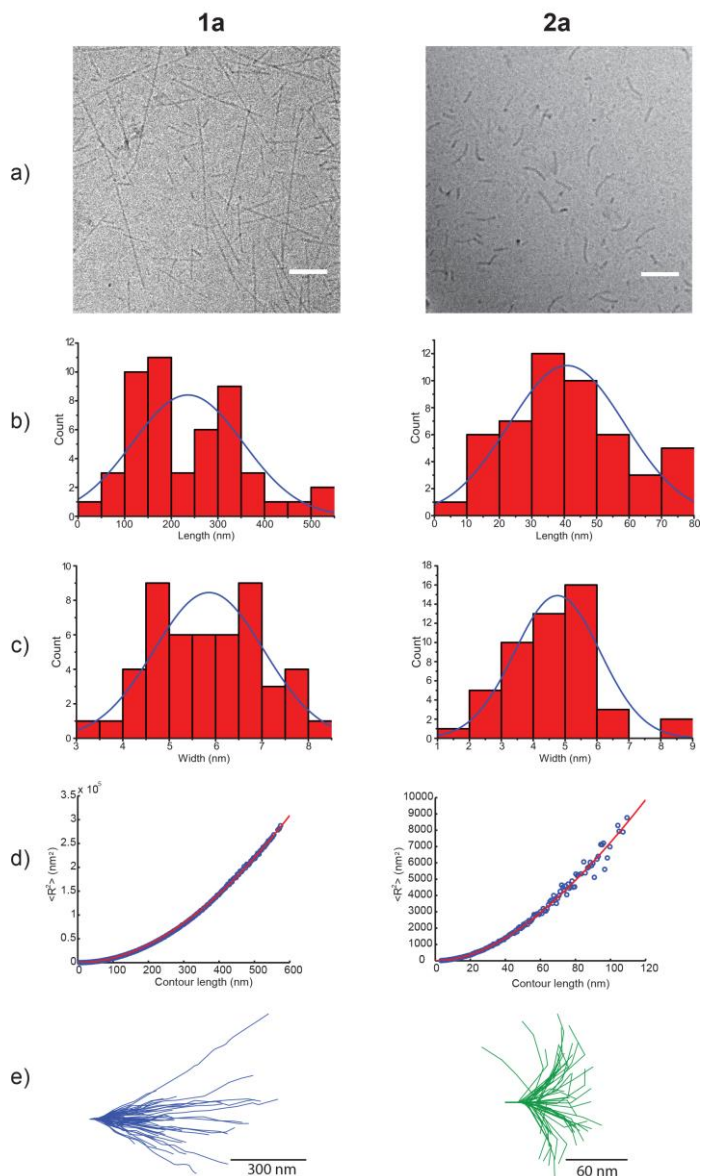


Figure 3.2. (a) Cryo-TEM images of **1a** (left) and **2a** (right) in aqueous solution (580 μM) after overnight equilibration. Scale bar: 100 nm. (b) Histograms of length distributions of **1a** (left) and **2a** (right) ($N = 50$, with average lengths of 235 ± 118 nm for **1a**, and 41 ± 18 nm for **2a**). (c) Histograms of width distributions of **1a** (left) and **2a** (right) ($N = 50$, with average widths of 5.8 ± 1.2 nm for **1a**, and 4.8 ± 1.3 nm for **2a**) (d) End-to-end distance plots (R^2) as function of contour length for **1a** (left) and **2a** (right), respectively, determined by cryo-TEM (blue open circles). Least-square fits are shown as red lines. (e) Fiber contours of **1a** (left) and **2a** (right) analyzed from cryo-TEM images, where initial tangents were aligned (contour lengths of 252 ± 116 nm for **1a** and 77 ± 17 nm for **2a**).

intermolecular hydrogen bonding geometries and aromaticity gain in synthons on the self-assembly mode “tug-of-war” of oxo- and thio-squaramide bolaamphiphiles. Despite the different hydrogen bonding arrangements of oxo- versus thio- squaramide synthons, computations suggest that both modes of self-assembly enhance the aromatic character of the squaramides, leading to stronger intermolecular interactions between the monomers, and increased structural rigidity in the respective supramolecular polymers.

3.3 Results and discussion

Synthesis and characterization of squaramide-based bolaamphiphiles. The molecular design of the squaramide-based bolaamphiphiles **1** and **2** consists of two squaramide synthons embedded within a hydrophobic core consisting of alkyl chains and surrounded by oligo(ethylene glycol)s to drive their nanophase segregation and one-dimensional self-assembly in water (see Figure 3.1c). In the original design of **1a**,²⁵ activation of the poly(ethylene glycol) by 1,1-carbonyldiimidazole was used for coupling to the hydrophobic spacer because of its synthetic facility, but to eliminate any effects imparted by the formed carbamate on the self-assembly an identical molecule bearing an ether between these domains was also synthesized and compared. The non-carbamate derivative **1b** was prepared by an alternate synthetic protocol (Scheme S3.1 and SI), giving moderate yields after reverse phase column chromatography. Thio-analogues **2a** and **2b** were prepared by reacting **1a** and **1b**, respectively, with pentathiodiphosphorus(V) acid-P,P'-bis(pyridinium betaine) in acetonitrile at room temperature to exclusively thionate the carbonyl groups of the squaramide moieties (Scheme S3.2);³⁶ reverse-phase column chromatography provided good yield for this step (89% **2a**, 72% **2b**). Carbon-13 nuclear magnetic resonance (¹³C-NMR) showed a downfield shift of $\Delta\delta \approx 20$ ppm of the C=S of the thiosquaramide compared to the C=O signal and a $\Delta\delta \approx 2-4$ ppm of the C=C of the cyclobutadione ring. The identity and purity of the proposed compounds were confirmed by a combination of techniques, including ¹H-NMR, ¹³C-NMR, LC-MS and ATR-FTIR (see Figure S3.1 and S3.2).

Monomer 2 forms shorter and more flexible supramolecular polymers than 1 in water. Cryogenic transmission electron microscopy (cryo-TEM) and small-angle X-ray scattering (SAXS) experiments probed the morphology and internal structure of the squaramide-based supramolecular polymers in water, showing surprisingly different aggregate morphologies and were thus suggestive of a distinct mode of self-assembly for the oxosquaramides and thiosquaramides in their respective fibers. Both **1a** and **1b** resulted in high-aspect-ratio fibers with lengths of 235 ± 118 and 246 ± 176 nm, respectively (Figures 3.2a, 3.2b, S3.6 and S3.7). In contrast, the thionated **2a** and **2b** were five to ten times shorter, displaying rod-like structures with lengths of 41 ± 18 and 24 ± 27 nm, respectively (Figure 3.2a, 3.2b, S3.6 and S3.7). The oxosquaramide supramolecular polymers (**1a**: 5.8 ± 1.2 nm, **1b**: 5.7 ± 1.2 nm) were also slightly thicker than the thiosquaramide derivatives (**2a**: 4.8 ± 1.3 nm and **2b**: 3.9 ± 1.1 nm) (Figure 3.2c and S3.7). Overall, by comparison of the molecules with and without the peripheral carbamates by cryo-TEM, these results suggest that the squaramide synthons are largely responsible for the observed self-assembled structures.

Statistical analyses of the cryo-TEM images with respect to the shape fluctuations of the supramolecular polymer structures suggest that **1a** forms long, rigid high-aspect ratio fibers, while **2a** forms short, flexible rod-like structures. Tracking of the contour lengths of the fibrillar assemblies using the Easyworm software³⁷ provided values of 252 ± 116 nm for **1a** and 77 ± 17 nm for **2a** (Figure 3.2d-e). Fig. 3.2d displays the mean square end-to-end distance $\langle R^2 \rangle$ plots as a function of contour length for the fiber (**1a**) and rod-like (**2a**) structures, respectively. The persistence length (P_l), which quantifies the stiffness of a semi-flexible polymer,³⁸ was determined from the $\langle R^2 \rangle$ by applying the worm-like chain model (WLC) (see supporting information, section 3.6.5).³⁷ Supramolecular polymers of **1a** displayed much larger P_l values (581 ± 76 nm)³⁷ compared to those of **2a** (47 ± 4 nm), and was thus suggestive of distinct mechanical properties for the oxo- versus thiosquaramide analogues. From P_l , the bending rigidity of the assembly of **1a** ($(2.4 \pm 0.3) \times 10^{-27}$ N·m²) was determined to be around 10-fold greater relative to that of **2a** ($(1.9 \pm 0.2) \times 10^{-28}$ N·m²).

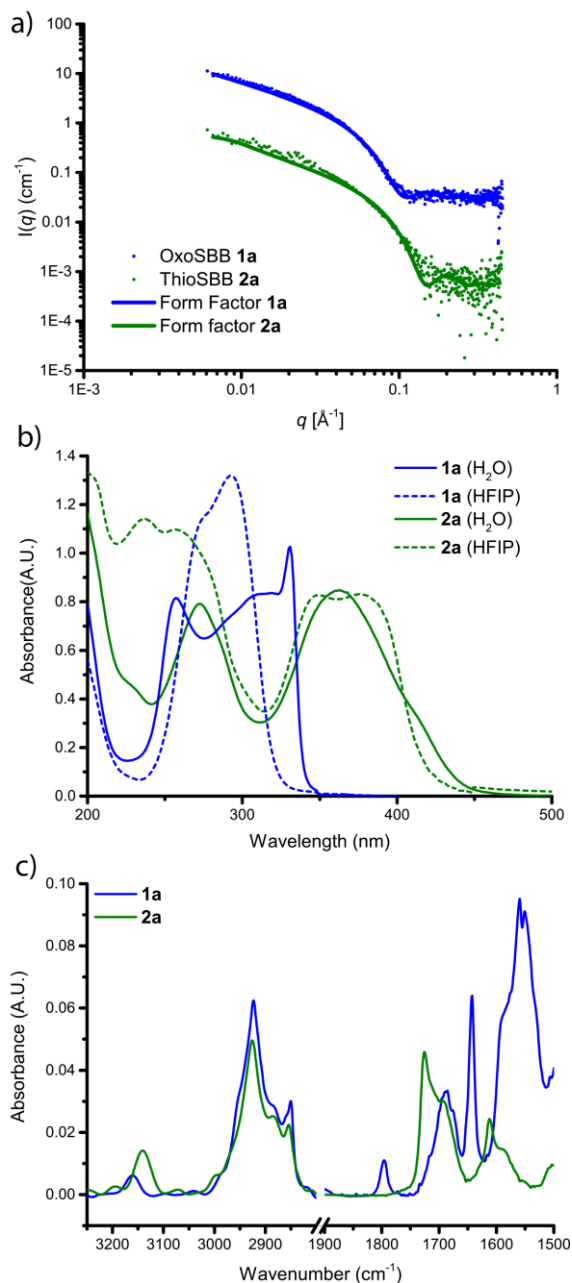


Figure 3.3. (a) Experimental SAXS profiles of **1a** and **2a** (5 mg mL^{-1}). The curves are modeled with a form factor for homogeneous and flexible homogenous cylinders for **1a** and **2a**, respectively. The blue curve is shifted vertically by multiplying with a factor of 10 to enable visualization of the two profiles. (b) UV-Vis spectrum of **1a** and **2a** in water and HFIP ($30 \mu\text{M}$). (c) IR spectrum recorded in the N-H region, amide I region and amide II in D_2O for both **1a** and **2a** (5.8 mM).

SAXS profiles provided further insight into the morphologies of the oxo- versus thiosquaramide-based supramolecular polymers. We previously found that self-assemblies of **1a** showed profiles with a q^{-1} slope in the low q regime (Figure 3.3a, blue line) characteristic of fiber-like objects.²⁵ The data was modelled with a form factor for homogeneous cylinders, yielding a cross-sectional radius (r_{cs}) of ~ 3.4 nm. From this data, the cross-sectional mass per unit length (M_L) of **1a** was determined (Table S3.1) yielding a comparable number of bolaamphiphiles within the cross-section as reported earlier by our group.²⁵ Supramolecular polymers of **2a** also displayed a q^{-1} slope at in the same region (Figure 3.3a, green line), but were better modelled with a form factor for flexible homogenous cylinders, resulting in an r_{cs} (~ 2.3 nm) on par with cryo-TEM images. From the M_L of **2a**, approximately 10-14 bolaamphiphiles per nm (see supporting information, section 3.6.6) were determined within the fiber cross-section. SAXS measurements of **1b** (q^{-1} slope) showed similar scattering profiles to **1a** with the carbamate moiety, whereas **2b** (Figure S3.8) displayed a significantly lower q -slope, indicating the coexistence of two morphologies. Consequently, the morphological differences and monomer packing found within the cross-section of **1** versus **2** clearly suggest that the mode of monomer self-assembly is different for the oxo- and thiosquaramide analogues.

Self-assembled monomers 1 and 2 show distinct spectroscopic signatures in water. Spectroscopic measurements, namely UV-Vis and IR, were used to shed light into the effect of self-assembly on the squaramide synthon and the self-assembly of the squaramide monomers at a molecular level. The UV-Vis spectrum of **1a** in water presents two absorption maxima at 255 nm and 329 nm, corresponding to the monomers self-assembled into a supramolecular polymer, and a broad band between these maxima belonging to the depolymerized fraction (Figure 3.3b, solid blue line). When **1a** is dissolved in hexafluoroisopropanol (HFIP), a low dielectric solvent known to effectively disrupt hydrogen bonds,³⁹⁻⁴¹ the two maxima start to coalesce, superimposing with the monomer band (Figure 3.3b, dotted blue line). Similar trends were observed for monomer **1b** in both conditions (Figure S3.11). UV-Vis spectra for the thiosquaramide analogs display the

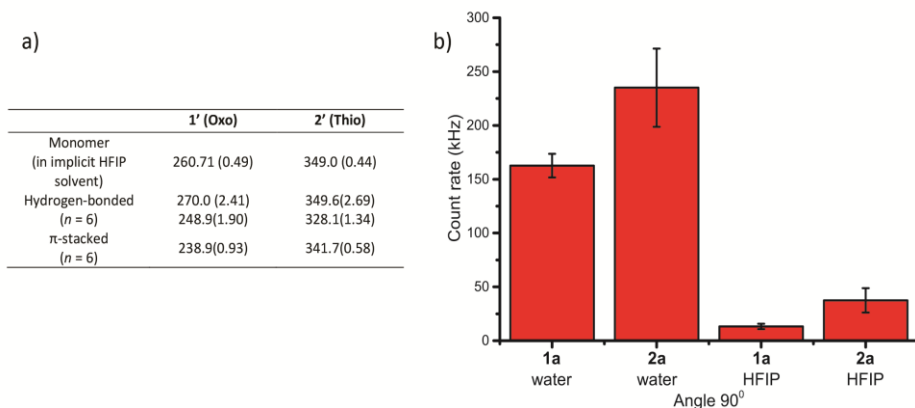


Figure 3.4. (a) Table with computed UV-Vis absorptions (λ , in nm) for the monomers, “head-to-tail” hexamers, and “stacked” hexamers of **1'** and **2'** in implicit solvation in a low dielectric solvent at IEF-PCM-M06-2X/6-311+G(d,p). Only transitions with oscillator strengths > 0.35 are listed (see values in parenthesis). (b) Scattered intensity (kHz) of samples of **1a** and **2a** in water and HFIP at the same concentration (580 μ M).

opposite trend in water, with **2a** showing bands with maxima at 363 nm and 272 nm (Figure 3.3b, solid green line); both are red-shifted in comparison to **1a**. Upon dissolving monomers of **2a** in HFIP, both bands at 272 and 363 nm are split into two peaks each at 258 and 237 nm, and 349 and 377 nm (Figure 3.3b, green dotted line), respectively. Similar trends in the UV-Vis spectra were observed for **2b** in both conditions (Figure S3.12).

To better understand the origin of the spectral differences in the two monomers in water and HFIP, TD-DFT computations were executed for models of N-methyl-oxosquaramide (**1'**) and N-methyl-thiosquaramide (**2'**) probing two potential aggregation modes for each: “head-to-tail” and “stacked.” UV absorption peaks in the 250 to 400 nm region were computed for the isolated monomers and self-assembled hexamers of **1'** and **2'** in implicit solvation at a low dielectric constant ($\epsilon < 20$, see supporting information, section 3.6.8) at IEF-PCM-M06-2X/6-311+G(d,p) to model **1** and **2** in their polymerized and depolymerized states (see table in Figure 3.4). Computed UV spectra revealed that when **1'** self-assembles in a “head-to-tail” mode, two coalescing peaks for the monomer at 259.1 and 258.7 nm, corresponding to the HOMO \rightarrow LUMO and HOMO \rightarrow LUMO+1 transitions respectively, become largely separate in the hexamer at 274.2

and 254.5 nm. These results are consistent with the experimentally obtained UV-Vis spectra for **1a** and **1b** in water (Figure 3.3b, blue solid line) and HFIP (Figure 3.3b, blue dotted line). On the other hand, when **2'** self-assembles in a “stacked” mode, the two peaks for the monomer at 347.4 and 336.1 nm, corresponding to the HOMO → LUMO and HOMO → LUMO+1 transitions respectively, coalesce upon oligomerization into peaks at 342.9 and 340.1 nm. These results are consistent with the experimentally obtained UV-Vis spectra for **2a** and **2b** in water (Figure 3.3b, green solid line) and HFIP (Figure 3.3b, green dotted line). For comparison, the computed UV results of the alternate self-assembly modes, i.e., “stacked” for **1'** and “head-to-tail” for **2'**, did not correlate with the experimentally observed trends (see data in Figure 3.4a). Hence, distinct UV-Vis spectra recorded for **1** and **2** are connected to their unique self-assembly modes that enable polarization of the squaramide motif.

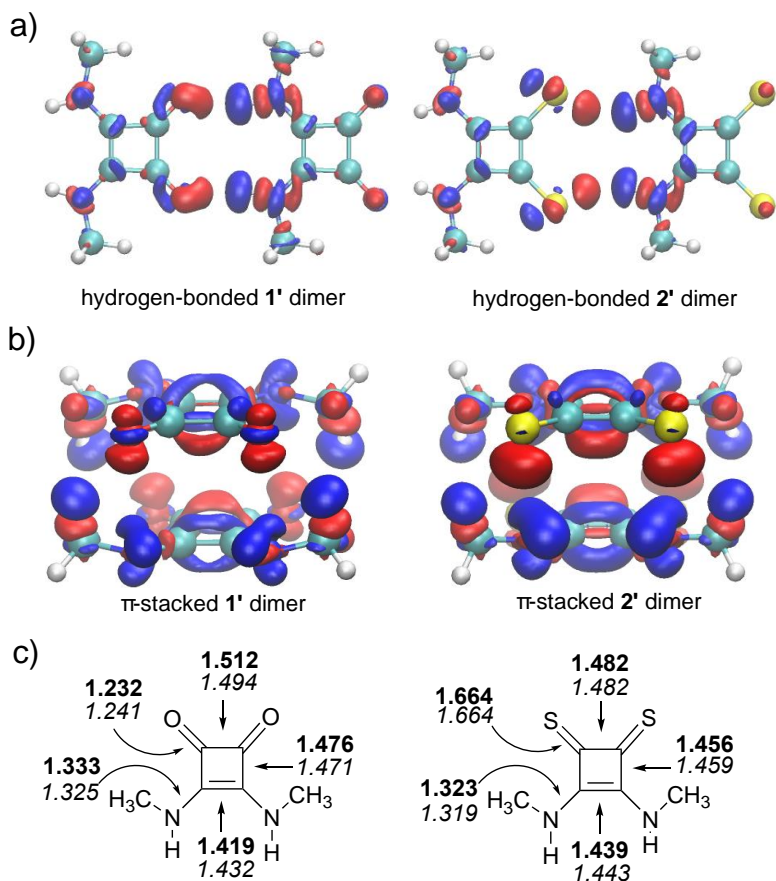


Figure 3.5. Computed electron density difference (EDD) maps for the (a) “head-to-tail” **1'** and **2'** dimers (note larger lobes on **1'**), and (b) “stacked” **1'** and **2'** dimers (note larger lobes on **2'**). Blue indicates electron density loss, red indicates electron density gain. (c) Computed geometries in implicit solvation for the isolated monomers of **1'** and **2'** (bond distances in Å, values in bold font), the “head-to-tail” hexamer of **1'** (left, averaged bond distances for each of the monomeric units, values in italics font), and the “stacked” hexamer of **2'** (right, averaged bond distances for each of the monomeric units, values in italics font).

Static light scattering (SLS) measurements of monomers **1a** and **2a** (Figure 3.4b) were performed in order to support their respective polymerization in water and depolymerization in HFIP solution. Scattered light intensities of supramolecular polymers of **1a** and **2a** indicated the presence of large objects in solution. When **1a** and **2a** were dissolved in HFIP, a 10-fold decrease in scattering intensity was recorded, consistent with the

depolymerization of the squaramide-based supramolecular polymers through solvation of the bolaamphiphiles and simultaneous disruption of hydrogen-bonding.

To confirm the role of hydrogen bonding in the self-assembly of the oxo- and thiosquaramides, infrared spectra were obtained for **1** and **2** in both D₂O and HFIP-d₂. In D₂O, **1a** showed asymmetric and symmetric C=O stretches at 1642, 1687, and 1676 cm⁻¹ for the squaramide and carbamate moieties, N–H stretches at 3162 cm⁻¹, and a small broad ring breathing band at 1796 cm⁻¹ (Figure 3.3c, blue). When **1a** was dissolved in HFIP-d₂, the C=O and ring breathing bands were shifted to higher wavenumbers by 10–15 cm⁻¹, with the latter indicative of greater ring bond length alternation in the squaramide moieties upon depolymerization; the N–H bands were not visible due to their likely overlap with stretches in the O–H region. For **2a**, C=O stretches at 1687 and 1676 cm⁻¹ were recorded for the carbamate moieties and an intense ring-breathing peak at 1726 cm⁻¹ (Figure 3.3c, green). The C=S stretches were expected to appear at the fingerprint region due to the heavier sulfur atom in the C=S bond comparison to the C=O, but could not be assigned due to their overlap with other bands of higher intensity. Additionally, compared to **1a**, the N–H stretches of **2a** were red-shifted to 3142 cm⁻¹ and of increased in intensity. When **2a** was dissolved in HFIP-d₂, the intense ring-breathing band was shifted towards lower wavenumbers by close to 20 cm⁻¹, and is consistent with shifts in the computed ring breathing frequencies for the **2'** monomer (at 1757 cm⁻¹) versus “stacked” **2'** hexamer (at 1774 cm⁻¹). In HFIP-d₂, the shift of the thiosquaramide N–H stretch confirmed disruption of the hydrogen-bond interaction between the monomers. Similar trends were observed for **1b** and **2b** (as well as **1a** and **2a**) in bulk and in solution (see Figure S3.1-5), respectively, except additional vibrations were recorded for the carbamate moieties. Key features of the IR spectra agreed with the computed IR vibrational modes of **1'** and **2'** as well as their self-assembled hexamers in implicit solvation at a low dielectric constant (see general methods and Tables S3.6 and S3.7). The solution-phase IR results suggest that both **1** and **2** engage in hydrogen bonding upon self-assembly, but the self-assembled **1** displays more significant ring bond length equalization than **2**.

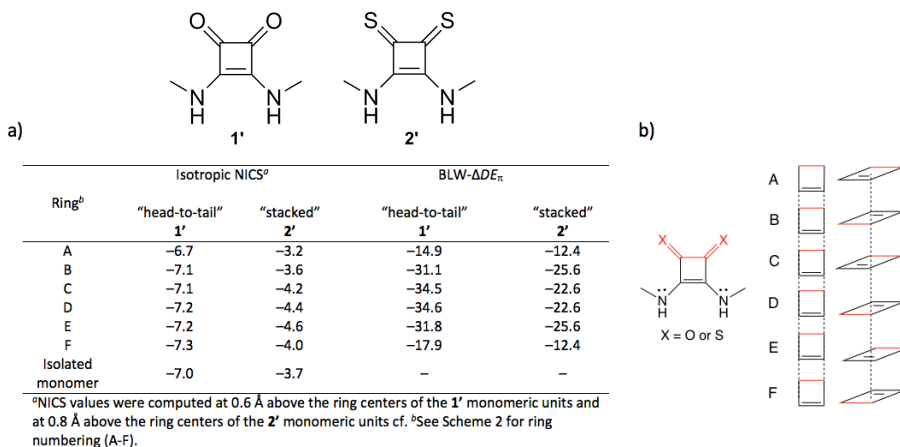


Figure 3.6. (a) Table with the computed isotropic NICS values (in ppm) and BLW- ΔDE_{π} values (in kcal/mol) for each of the monomer rings in the “head-to-tail” 1' hexamer and “stacked” 2' hexamer. More negative NICS values indicate greater aromaticity gain in the monomers upon self-assembly. All BLW- ΔDE_{π} values were computed at B3LYP/6-31G(d); more negative ΔDE_{π} values indicate greater cyclic π -electron delocalization gain in the monomers upon self-assembly. (b) Rings A to F in the “head-to-tail” and “stacked” hexamers of 1' and 2'.

Computational studies of aromaticity gain in oxo- and thioamidine supramolecular polymers. Density Functional Theory (DFT) computations of model “head-to-tail” and “stacked” hexamers of 1' and 2' were carried out to examine the competition between the different self-assembly modes. Single point energy calculations at the IEF-PCM-M06-2X/6-311+G(d,p) level (see supporting information, section 3.6.8) reveal a more negative averaged hydrogen bonding interaction energy (ΔE_{HB}) for the “head-to-tail” 1' hexamer (−10.77 kcal/mol) compared to that of the “stacked” 1' hexamer (−8.73 kcal/mol), indicating that the “head-to-tail” mode is favoured for 1' in water. Conversely, the computed averaged ΔE_{HB} for the “head-to-tail” 2' hexamer (−9.00 kcal/mol) was significantly lower relative to that of the “stacked” 2' hexamer (−12.99 kcal/mol), suggesting a dominant stacking mode for 2' in water. Accordingly, computed electron density difference (EDD) maps for the “head-to-tail” vs. “stacked” dimers of 1' and 2' show that C=O's form effective hydrogen bonding interactions with N–H's in the O lone-pair plane, but C=S's form stronger interactions with the N–H's at roughly 90° angles to the S lone-pair plane. As shown in Figure 3.5a, EDD maps for the “head-to-tail” 1' and 2' dimers show increased electron

density at the O/S's (indicated in red, electron density gain) and decreased electron density at the amine H's (indicated in blue, electron density loss); as expected by the stronger hydrogen bond acceptor ability of C=O, the "head-to-tail" **1'** dimer displays greater electron density change. In Figure 3.5b, EDD maps of the "stacked" **1'** and **2'** dimers also show increased electron density at the O/S's (in red) and decreased electron density at the general N–H region (in blue), suggestive of attractive noncovalent interactions between the stacks. The much greater electron density change for the "stacked" **2'** dimer is consistent with the ability of C=S to engage in less directional hydrogen bonding interactions.^{33,34} These findings further support that differences in the physical properties and spectroscopic features of the supramolecular polymers of **1** versus **2** likely arise from their preferred self-assembly modes.

Computed geometries for the monomers and hexamers of **1'** and **2'** at the IEF-PCM-B3LYP-D3/6-31+G(d) level show that the ring bonds of **1'** (Figure 3.5c, left, values in bold font) become more bond length equalized (i.e., increased aromatic character) upon self-assembly in the "head-to-tail" **1'** hexamer (values in italics font); all of the single bonds shorten (by 0.005 to 0.018 Å) and the double bonds lengthen (by 0.009 to 0.013 Å). In contrast, the ring bonds of **2'** (Figure 3.5c, right, values in bold font) are altered to a lesser degree upon self-assembly in the "stacked" **2'** hexamer (values in italics font); the two C–N bonds shorten (by 0.004 Å) and the ring C=C bond lengthens (by 0.004 Å), but the C–C and C=S bonds exhibit little to no change (a zero to 0.003 Å change). Harmonic Oscillator Model of Electron Delocalization (HOMED) analyses⁴² confirm these observations, showing increased HOMED values when **1'** (0.329, HOMED value for isolated monomer) self-assembles into the "head-to-tail" **1'** hexamer (0.383, averaged HOMED values for six monomer units), while those of **2'** (0.447, isolated monomer) and the "stacked" **2'** hexamer (0.445, average for six monomer units) stay close. HOMED values range from 0 (non-aromatic) to 1 (fully aromatic compounds) and measure the degree of ring bond equalization in molecules as a criterion for aromaticity (see supporting information, section 3.6.10). These geometric features agree with the IR spectra of **1(a/b)** and **2(a/b)** in the solution phase, which suggest that the

geometries of oxo- and thiosquaramides change in opposite ways upon monomer self-assembly.

Computations based on the magnetic and energetic criteria of aromaticity revealed significant aromaticity gain in both the “head-to-tail” self-assembled monomers of **1'** and the “stacked” monomers of **2'**. Isotropic nucleus independent chemical shifts (NICS)^{43,44} were computed at 0.6 Å above each of the “head-to-tail” **1'** ring centers, and at 0.8 Å above each of the “stacked” **2'** ring centers (due to the more diffuse orbitals of the S atoms) to quantify the magnetic effects of aromaticity gain. As shown in the table in Figure 3.6, the computed isotropic NICS for both **1'** (NICS(0.6) = –7.0 ppm) and **2'** (NICS(0.8) = –3.7 ppm) become more negative in the “head-to-tail” **1'** hexamer (NICS(0.6) = –6.7 to –7.3 ppm) and “stacked” **2'** hexamer (NICS(0.8) = –3.2 to –4.6 ppm), documenting aromaticity gain in both monomers upon self-assembly.

Block-localized wavefunction (BLW) analyses⁴⁵ quantified the energetic effects of aromaticity gain in the “head-to-tail” hexamer of **1'** and the “stacked” hexamer of **2'** (see supporting information, section 3.6.10). The BLW method, the simplest variant of valence bond calculations, measures π -electron delocalization energies (DE_{π}) in molecules by comparing the energy of the fully delocalized wavefunction (Ψ_{deloc}) of a molecule to that of its hypothetical π -electron localized wavefunction (Ψ_{loc}) in which all π -electron delocalization effects are “turned off”: $DE_{\pi} = \Psi_{\text{deloc}} - \Psi_{\text{loc}}$ (i.e., a more negative DE_{π} value indicates more π -electron delocalization in a molecule). The computed DE_{π} difference between the isolated monomers (e.g., **1'** and **2'**) versus “head-to-tail” or “stacked” monomers provides a measure of the extra gain in π -electron delocalization in monomers upon self-assembly; $\Delta DE_{\pi} = DE_{\pi}$ (“head-to-tail” or “stacked” monomer) – DE_{π} (monomer) (i.e., a more negative ΔDE_{π} value indicates more π -conjugation gain upon “head-to-tail” hydrogen-bonding or “stacked” hydrogen-bonding of the monomer). For cyclic π -conjugated monomers, like **1'** and **2'**, large negative ΔDE_{π} values suggest enhanced aromatic character in the self-assembled monomer (see supporting information, section 3.6.10 and Figure 3.6a). Remarkably, the computed ΔDE_{π} values for each of the monomers in

the “head-to-tail” **1'** hexamer (averaged $\Delta DE_{\pi} = -27.5$ kcal/mol) and the “stacked” **2'** hexamer (averaged $\Delta DE_{\pi} = -20.6$ kcal/mol) are substantial, and suggest significant aromaticity gain upon self-assembly through hydrogen bonding (Table S3.2 for more details). These computations suggest that in low dielectric environments, such as in the hydrophobic core of a supramolecular polymer, aromaticity gain can be considered as an important driving force when combined with hydrogen-bonding to direct the self-assembly of supramolecular polymers.

3.4 Conclusions

Here I demonstrate that oxosquaramide and thiosquaramide monomers self-assemble into surprisingly different fibrillar morphologies in water: oxosquaramide-based bolaamphiphiles form long, rigid fibrillar architectures, while the thio-analogues form short, flexible rod-like structures. Evidence based on spectroscopic measurements and computational analyses revealed that oxosquaramides self-assemble into a “head-to-tail” arrangement by aligning their hydrogen bond donors (N–H’s) and acceptors (C=O’s) along the squaramide ring plane, while thiosquaramides prefer antiparallel “stacked” configurations in which the N–H’s of each unit are stacked above and below the C=S’s of an adjacent layer and interact through C=S \cdots H hydrogen bonding with a close to 90° C=S \cdots H angle, suggesting that the hydrogen bond in the oxosquaramides have a preferential alignment parallel to the fiber axes, while thiosquaramides might not benefit of this alignment resulting in a decrease of the length and stiffness of the aggregate. Based on IR measurements, the self-assembled oxosquaramides displayed distinct bond length equalization, whereas ring bond distances of the self-assembled thiosquaramides were altered to a lesser degree. However, computations revealed that polarization of both monomers in the “head-to-tail” and “stacked” self-assembly modes occurs through hydrogen bonding, thereby increasing the aromatic character of both squaramide synthons. These findings further suggest that changes in the aromatic characters of hydrogen-bonding synthons can be used to “fine-tune” the intermolecular interactions between monomers, with potent effects on their mode of supramolecular polymerization. I emphasize that beside the often-used checklist for

controlling hydrogen bonding interactions,⁸⁻¹⁰ *aromaticity gain* also should be considered in the molecular designs of self-assembling monomers for supramolecular polymers, and more broadly in supramolecular chemistry.

3.5 References

- (1) Aida, T., Meijer, E. W. & Stupp, S. I. *Science*, **2012**, 335 (6070), 813–817.
- (2) Appel, E. A., del Barrio, J., Loh, X. J. & Scherman, O. A. *Chem. Soc. Rev.*, **2012**, 41 (18), 6195–214.
- (3) Rieth, S., Baddeley, C. & Badjic, J. D. *Soft Matter*, **2007**, 3 (4), 137.
- (4) Krieg, E., Bastings, M. M. C., Besenius, P. & Rybtchinski, B. *Chem. Rev.*, **2016**, 116 (4), 2414–2477.
- (5) de Greef, T. F. A. & Meijer, E. W. *Nature*, **2008**, 453 (7192), 171–173.
- (6) Thiele, J., Ma, Y., Bruekers, S. M. C., Ma, S. & Huck, W. T. S. *Adv. Mater.*, **2014**, 26 (1), 125–148.
- (7) Webber, M. J., Appel, E. A., Meijer, E. W. & Langer, R. Supramolecular biomaterials. *Nat. Mater.*, **2015**, 15 (1), 13–26.
- (8) Fernandez-Castano Romera, M., Lafleur, R. P. M., Guibert, C., Voets, I. K., Storm, C. & Sijbesma, R. P. *Angew. Chemie. Int. Ed.*, **2017**, 56 (30), 8771–8775.
- (9) Obert, E., Bellot, M., Bouteiller, L., Andrioletti, F., Lehen-Ferrenbach, C. & Boué, F. *J. Am. Chem. Soc.*, **2007**, 129 (50), 15601–15605.
- (10) Park, T. & Zimmerman, S. C. *J. Am. Chem. Soc.*, **2006**, 128 (35), 11582–11590.
- (11) Wilson, A. J. *Soft Matter*, **2007**, 3 (4), 409.
- (12) Shen, Z., Wang, T. & Liu, M. *Chem. Commun.*, **2014**, 50 (17), 2096–9.

Chapter 3

- (13) Leenders, C. M. A., Baker, M. B., Pijpers, I. A. B., Lafleur, R. P. M., Albertazzi, L., Palmans, A. R. A. & Meijer, E. W. *Soft Matter*, **2016**, *12* (11), 2887–2893.
- (14) Baram, J., Weissman, H., Tidhar, Y., Pinkas, I. & Rybtchinski, B. *Angew. Chem. Int. Ed.*, **2014**, *53* (16), 4123–6.
- (15) Nakano, Y., Markvoort, A. J., Cantekin, S., Filot, I. A. W., Ten Eikelder, H. M. M., Meijer, E. W. & Palmans, A. R. A. *J. Am. Chem. Soc.*, **2013**, *135*, 16497–16506.
- (16) Lloyd, G. O. & Steed, J. W. *Nat. Chem.*, **2009**, *1*, 437–442.
- (17) Siddiqui, S. & Spano, F. *Chem. Phys. Lett.*, **1999**, *308*, 99–105.
- (18) Rybtchinski, B. *ACS Nano*, **2011**, *5*, 6791–818.
- (19) Rudolph, T., Kumar Allampally, N., Fernández, G. & Schacher, F. H. *Chem. Eur. J.*, **2014**, *20*, 13871–13875.
- (20) Jalani, K., Dhiman, S., Jain, A. & George, S. J. *Chem. Sci.*, **2017**, *8*, 6030–6036.
- (21) Wu, J. I., Jackson, J. E. & Schleyer, P. V. R. *J. Am. Chem. Soc.*, **2014**, *136*, 13526–13529.
- (22) Kakeshpour, T., Wu, J. I. & Jackson, J. E. *J. Am. Chem. Soc.*, **2016**, *138*, 3427–3432.
- (23) Anand, M., Fernández, I., Schaefer, H. F. & Wu, J. I. *J. Comput. Chem.*, **2016**, *37*, 59–63.
- (24) Kakeshpour, T., Bailey, J. P., Jenner, M. R., Howell, D. E., Staples, R. J., Holmes, D., Wu, J. I., Jackson, J. E. *Angew. Chem. Int. Ed.*, **2017**, *56*, 9842.
- (25) Saez Talens, V., Englebienne, P., Trinh, T. T., Noteborn, W. E. M., Voets, I. K. & Kieltyka, R. E. *Angew. Chemie. Int. Ed.*, **2015**, *54* (36), 10502–10506.

- (26) Soberats, B., Martínez, L., Sanna, E., Sampedro, A., Rotger, C. & Costa. *Chem. Eur. J.*, **2012**, *18*, 7533–7542.
- (27) López, C., Ximenis, M., Orvay, F., Rotger, C. & Costa, A. *Chem. Eur. J.*, **2017**, *23*, 7590–7597.
- (28) Ian Storer, R., Aciro, C. & Jones, L. H. *Chem. Soc. Rev.*, **2011**, *40*, 2330.
- (29) Alemán, J., Parra, A., Jiang, H. & Jørgensen, K. A. *Chem. Eur. J.*, **2011**, *17*, 6890–6899.
- (30) Quiñonero, D., Prohens, R., Garau, C., Frontera, A., Ballester, P., Costa, A. & Deyà, P. M. *Chem. Phys. Lett.*, **2002**, *351*, 115–120.
- (31) Busschaert, N., Elmes, R. B. P., Czech, D. D., Wu, X., Kirby, I. L., Peck, E. M., Hendzel, K. D., Shaw, S. K., Chan, B., Smith, B. D., Jolliffe, K. A. & Gale, P. A. *Chem. Sci.*, **2014**, *5*, 3617–3626.
- (32) Lee, H. J., Choi, Y. S., Lee, K. B., Park, J. & Yoon, C. J. *J. Phys. Chem. A.*, **2002**, *106*, 7010–7017.
- (33) Lenthall, J. T., Foster, J. A., Anderson, K. M., Probert, M. R., Howard, J. A. K. & Steed, J. W. *CrystEngComm*, **2011**, *13*, 3202–3212.
- (34) Custelcean, R., Engle, N. L. & Bonnesen, P. V. *CrystEngComm*, **2007**, *9*, 452.
- (35) Allen, F. H., Bird, C. M., Rowland, R. S. & Raithby, P. R. *Acta Crystallogr. Sect. B Struct. Sci.*, **1997**, *53*, 680–695.
- (36) Bergman, J., Pettersson, B., Hasimbegovic, V. & Svensson, P. H. *J. Org. Chem.*, **2011**, *76*, 1546–1553.
- (37) Lamour, G., Kirkegaard, J. B., Li, H., Knowles, T. P. & Gsponer, J. *Source Code Biol. Med.*, **2014**, *9*, 16.
- (38) Makky, A., Bousset, L., Polesel-Maris, J. & Melki, R. *Sci. Rep.*, **2016**, *6*, 37970.

- (39) Leenders, C. M. A., Albertazzi, L., Mes, T., Koenigs, M. M. E., Palmans, A. R. A., Meijer, E. W. *Chem. Commun.*, **2013**, 49, 1963–1965.
- (40) Korevaar, P. A., Newcomb, C. J., Meijer, E. W., & Stupp, S. I. *J. Am. Chem. Soc.*, **2014**, 136, 8540–8543.
- (41) Boekhoven, J., Brizard, A. M., van Rijn, P., Stuart, M. C. A., Eelkema, R., & van Esch, J. H. *Angew. Chemie. Int. Ed.*, **2011**, 50, 12285–12289.
- (42) Raczyńska, E. D., Hallman, M., Kolczyńska, K. & Stępniewski, T. M. *Symmetry (Basel)*, **2010**, 2, 1485–1509.
- (43) Chen, Z., Wannere, C. S., Corminboeuf, C., Puchta, R. & Schleyer, P. von R. *Chem. Rev.*, **2005**, 105, 3842–3888.
- (44) Schleyer, P. V. R., Maerker, C., Dransfeld, A., Jiao, H. & Van Eikema Hommes, N. J. R. *J. Am. Chem. Soc.*, **1996**, 118, 6317–6318.
- (45) Mo, Y., Song, L. & Lin, Y. *J. Phys. Chem. A.*, **2007**, 111, 8291–8301.
- (46) Frisch, M. J., Trucks, G. W., Schlegel, H. B., Scuseria, G. E., Robb, M. A., Cheeseman, J. R., Scalmani, G., Barone, V., Mennucci, B., Petersson, G. A., Nakatsuji, H., Caricato, M., Li, X., Hratchian, H. P., Izmaylov, A. F., Bloino, J., Zheng, G., Sonnenberg, J. L., Hada, M., Ehara, M., Toyota, K., Fukuda, R., Hasegawa, J., Ishida, M., Nakajima, T., Honda, Y., Kitao, O., Nakai, H., Vreven, T., Montgomery, J. A., Jr., Peralta, J. E., Ogliaro, F., Bearpark, M., Heyd, J. J., Brothers, E., Kudin, K. N., Staroverov, V. N., Keith, T., Kobayashi, R., Normand, J., Raghavachari, K., Rendell, A., Burant, J. C., Iyengar, S. S., Tomasi, J., Cossi, M., Rega, N., Millam, J. M., Klene, M., Knox, J. E., Cross, J. B., Bakken, V., Adamo, C., Jaramillo, J., Gomperts, R., Stratmann, R. E., Yazyev, O., Austin, A. J., Cammi, R., Pomelli, C., Ochterski, J. W., Martin, R. L., Morokuma, K., Zakrzewski, V. G., Voth, G. A., Salvador, P., Dannenberg, J. J., Dapprich, S., Daniels, A. D., Farkas, Ö., Foresman, J. B., Ortiz, J. V., Cioslowski, J., Fox, D. J. *Gaussian 09, revision D.01*, Gaussian, Inc., Wallingford, CT, **2013**.

- (47) Schmidt, M. W., Baldrige, K. K., Boatz, J. A., Elbert, S.T., Gordon, M. S., Jensen, J. H., Koseki, S., Matsunaga, N., Nguyen, K. A., Su, S., Windus, T. L., Dupuis, M., Montgomery J. A. *J. Comput. Chem.*, **1993**, *14*, 1347–1363.

3.6 Supporting Information

3.6.1 Materials

All reagents and chemicals were obtained from commercial sources at the highest purity available and used without further purification. O-methylundecaethylene glycol was obtained from Polypure and Broadpharm. Palladium on matrix activated carbon, triethylsilane and all other commercially available chemicals were purchased from Sigma Aldrich. Deuterated chloroform was purchased from Euriso-top and Milli-Q water was employed for all the experiments.

3.6.2 General methods

Cryo transmission electron microscopy (Cryo-TEM). Cryogenic TEM (cryo-TEM) samples were imaged with a Tecnai F20 equipped with a field emission gun (FEI company) at 200 keV using a Gatan UltraScan camera (Gatan company) with a defocus between -4 and -10 μm . Samples were prepared by applying a 3 μL sample of **1(a/b)** or **2(a/b)** in water to a glow-discharged Quantifoil R2/2 holey carbon film or 300 mesh copper grid with a lacey-carbon support film (Supplier-Electron Microscopy Sciences). Excess liquid was blotted off for 1 second and plunge-frozen in liquid ethane using a Leica EMGP. The length and width of the aggregates were measured using Fiji software (<https://fiji.sc/> - TIA reader plugin). The size distribution was obtained by measuring the length and the width of 50 fibers per sample. Details on the calculation of the persistence length (P_i) and bending rigidity (κ) are given in Supplementary Note 2. The resulting assemblies of **1a** and **2a** were tracked by using the Easyworm software.³⁷

Small angle X-ray scattering (SAXS). Small angle X-ray scattering measurements (SAXS) were carried out on a SAXSLAB GANESHA 300 XL SAXS system equipped with a GeniX 3D Cu Ultra Low Divergence micro focus sealed tube source producing X-rays with a wavelength $\lambda = 1.54 \text{ \AA}$ at a flux of 1×10^8 ph/s and a Pilatus 300K silicon pixel detector with 487×619 pixels of $172 \mu\text{m} \times 172 \mu\text{m}$ in size, which is placed at two sample-to-detector distances of 713 and 1513 mm respectively to access a q -range of $0.06 \leq q \leq 0.44 \text{ \AA}^{-1}$ with $q = 4 \pi / \lambda (\sin\Theta/2)$. Samples of 4 and 5 mg mL^{-1} concentration

were prepared the night before measurement and contained at room temperature in 2 mm quartz capillaries (Hilgenberg GmbH) during the measurements. Further details are described in Supplementary Note 3.

Ultraviolet-visible spectroscopy (UV-Vis). Absorption spectra were acquired using a Cary 300 UV-Vis spectrophotometer. All measurements were performed at room temperature using a quartz cuvette with a path length of 1 cm scanning from 200 to 500 nm. Samples were prepared by dissolving the analyte in the corresponding solvent to reach a final concentration of 30 μM . Samples were left to equilibrate overnight prior measurement.

Infrared spectroscopy (IR). IR spectra in the solid state were recorded on a Perkin Elmer UATR Two FT-IR spectrometer set to a resolution of 4 cm^{-1} . IR spectra in the solution state were recorded using a Bio-Rad Excalibur spectrometer equipped with a nitrogen cooled MCT detector. A liquid transmission cell with CaF_2 windows and a fixed nominal path length of 50 μm was used. Solution phase measurements were performed using D_2O and HFIP- d_2 at room temperature with a final concentration of 5.8 mM for all the samples. After preparation, samples were equilibrated overnight prior to measurement. Spectra were recorded at room temperature, with a resolution of 1 cm^{-1} averaged over 128 scans. The final absorbance spectra was expressed in terms of absorbance and corrected by manual subtraction of a water vapor spectrum. Baseline subtraction was performed using Origin 9.1 software.

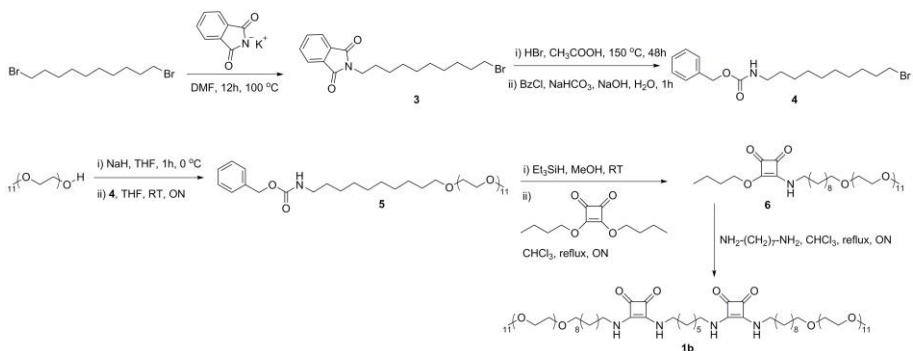
Static light scattering (SLS). SLS experiments were conducted on an ALV/CGS-3 MD-4 compact goniometer system equipped with a multiple Tau digital real time correlator (ALV-7004) and a solid-state laser ($\lambda = 532\text{ nm}$; 40 mW). All samples were prepared at a concentration of 580 μM and equilibrated overnight prior to measurement. Experiments covered scattering angles from 60 to 120°, averaged over 6 runs of 10 s each at room temperature.

Computational methods. Geometries of the **1'** and **2'** monomers, head-to-tail hexamers, and stacked hexamers were optimized in implicit solvation at $\epsilon = 16.7$ at the IEF-PCM-B3LYP-D3/6-31+G(d) level using ultrafine grid employing the Gaussian09 program.⁴⁶ "Head-to-tail" hexamers of **1'** and **2'** were optimized with C_{2v} symmetry constraint, based on an initial geometry where the N-H groups of each unit were hydrogen bonded to the C=O/S groups of a neighboring unit along the squaramide ring plane. "Stacked" hexamers of **1'** and **2'** were optimized with a constrained C_s symmetry, based on an initial geometry where the N-H groups of each unit were stacked above and below the C=O/S groups of a neighboring monomeric unit. Based on geometries optimized at the IEF-PCM-B3LYP-D3/6-31+G(d) level, single point hydrogen bonding interaction energies (ΔE_{HB}) of the "head-to-tail" and "stacked" hexamers of **1'** and **2'** were computed in implicit solvation at $\epsilon = 16.7$ at the IEF-PCM-M06-2X/6-311+G(d,p) level; ΔE_{HB} is the total electronic energy of a hexamer minus six times the total electronic energy of its monomeric units. Electron density difference (EDD) maps for the "head-to-tail" and "stacked" dimers of **1'** and **2'** were computed at the B3LYP-D3/6-31+G(d) level.

Due to the limited selection of dielectric constants available in Gaussian09 for frequency and TD-DFT calculations, computed IR, UV, and NICS analyses for the monomers and hexamers were performed in implicit solvation at $\epsilon = 8.5$ to mimic both the low dielectric environment of the HFIP solvent as well as the hydrophobic environment of the self-assembled polymers in water. IR vibrational frequencies were computed at the IEF-PCM-B3LYP-D3/6-31+G(d) level. TD-DFT calculations were performed at the IEF-PCM-M06-2X/6-311+G(d,p) level known to match well with experimental UV results. Isotropic nucleus independent chemical shifts (NICS)^{43,44} values were computed at 0.6 Å above the squaramide ring centers and at 0.8 Å above the thiosquaramide rings centers, at the IEF-PCM-PW91/IGLOIII level. Block-localized wavefunction (BLW)⁴⁵ computations were performed in implicit solvation at $\epsilon = 8.5$ at the PCM-B3LYP/6-31G(d) level with the GAMESS 2013-R1 program⁴⁷ (see full details for the BLW method in section 3.6.10).

3.6.3 Synthetic routes

3.1 Synthesis of compound 1b



Scheme S3.1. Synthetic route for compound 1b

Synthesis of 3

1,10-dibromodecane (20.0 g, 66.7 mmol) was added to potassium phthalimide (2.5 g, 13.4 mmol) in DMF (20 mL), resulting in a cloudy suspension that was refluxed for 12 h. Once the solvent was removed by evaporation under vacuum, the reaction mixture was purified by column chromatography (ethyl acetate/petroleum ether, 1:40). The resulting product was concentrated in a rotary evaporator, followed by drying with a gentle stream of air overnight to yield a white solid.

Yield: 4.1 g, 83 %. ¹H-NMR (δ_H[ppm], CDCl₃, 500 MHz): 7.88-7.84 (m, 2H), 7.75-7.71 (m, 2H), 3.72-3.68 (t, 2H), 3.44-3.40 (t, 2H), 1.90-1.83 (m, 2H), 1.71-1.65 (m, 2H), 1.45-1.29 (m, 12H). ¹³C-NMR (δ_C[ppm], CDCl₃, 125 MHz): 168.46, 133.90, 132.20, 123.18, 38.07, 34.13, 32.87, 29.40, 29.38, 29.17, 28.77, 28.63, 28.20, 26.87.

Synthesis of 4

Compound 3 (3.0 g, 8.1 mmol) was dissolved in acetic acid (10 mL), hydrogen bromide (48 %, 4 mL) was added and the mixture was refluxed at 150 °C for 48 h. The brown suspension was evaporated to dryness using a rotary evaporator followed by a gentle stream of air overnight. The deprotection of the phthalimide to yield the primary amine was followed by

Chapter 3

$^1\text{H-NMR}$ and $^{13}\text{C-NMR}$. The reaction was assumed to be quantitative by $^1\text{H-NMR}$ and the product was used without further purification.

$^1\text{H-NMR}$ (δ_{H} [ppm], CDCl_3 , 400 MHz): 8.04 (br s, 3H), 3.46-3.41 (t, 2H), 3.05 (m, 2H), 2.13-1.79 (m, 4H), 1.35-1.32 (m, 4H), 1.09-1.05 (m, 8H). $^{13}\text{C-NMR}$ (δ_{C} [ppm], CDCl_3 , 100 MHz): 40.29, 34.04, 32.88, 29.37, 29.31, 28.97, 28.77, 28.21, 27.53, 26.61.

Sodium bicarbonate (1.0 g, 12.0 mmol) in water (15 mL) was added to the deprotected primary amine, resulting in a foaming solution. The mixture was cooled to 0°C prior to the addition of benzyl chloroformate (2.3 mL, 16.1 mmol). A 1M solution of sodium hydroxide (3.5 mL, 3.5 mmol) was then added dropwise over 20 minutes and stirred overnight. The reaction mixture was extracted from the aqueous layer 5 times with chloroform (20 mL). The product was purified by column chromatography using petroleum ether/ethyl acetate, 9:1, and the solvents were removed using a rotary evaporator yielding a yellow solid.

Yield: 1.9 g, 63 %. $^1\text{H-NMR}$ (δ_{H} [ppm], CDCl_3 , 400 MHz): 7.37-7.28 (m, 5H), 5.11 (s, 2H), 4.88 (br s, 1H), 3.44-3.39 (m, 2H), 3.22-3.13 (m, 2H), 2.05-1.80 (m, 2H), 1.52-1.41 (m, 2H), 1.33-1.30 (m, 10H). $^{13}\text{C-NMR}$ (δ_{C} [ppm], CDCl_3 , 100 MHz): 156.03, 137.29, 128.29, 127.68, 127.64, 65.01, 40.13, 38.73, 29.35, 28.82, 28.72, 28.64, 28.46, 26.92, 26.18, 25.76.

Synthesis of 5

O-methyl-undecaethylene glycol (0.8 g, 1.6 mmol) was dissolved in tetrahydrofuran (5 mL) and cooled to 0°C . Sodium hydride (60 % in mineral oil) (55.7 mg, 2.3 mmol) was then added, resulting in vigorous foaming. The reaction mixture was stirred for one hour; then the ice bath was removed, compound **4** (0.9 g, 2.3 mmol) was added, and stirred overnight at room temperature. Purification of the product was performed by flash column chromatography on a C18 silica column with a gradient of 10-90% $\text{CH}_3\text{CN}/\text{H}_2\text{O}$ over 45 minutes. The purified product was concentrated using a rotary evaporator and lyophilized overnight to yield a white solid.

Yield: 30 %, 0.4 g. $^1\text{H-NMR}$ (δ_{H} [ppm], CDCl_3 , 400 MHz): 7.36-7.28 (m, 5H), 5.09 (s, 2H), 4.22-4.20 (m, 1H), 3.64-3.52 (m, 43H), 3.46-3.37 (m, 5H), 3.18-3.13 (m, 2H), 1.63-1.27 (m, 16H). $^{13}\text{C-NMR}$ (δ_{C} [ppm], CDCl_3 , 100 MHz): 128.56, 128.12, 72.00, 71.59, 70.62, 70.56, 70.11, 69.75, 66.61, 63.84, 59.08, 41.19, 30.02, 29.69, 29.52, 29.31, 26.79, 26.13. LC-MS: $t = 8.20$ min, m/z : 823.60 $[\text{M}+\text{H}]^+$.

Synthesis of 6

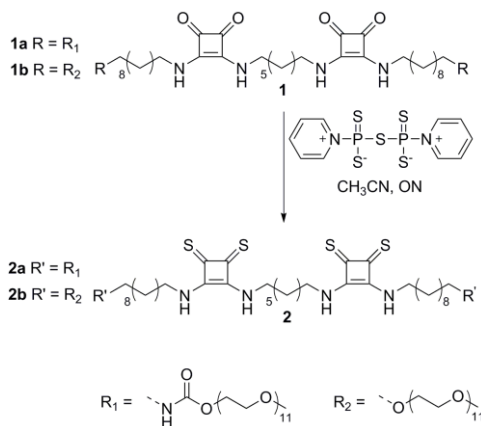
Compound **5** (0.4 g, 0.5 mmol) was dissolved in methanol (5 mL) with a catalytic amount of Pd/C, and degassed briefly with argon gas. Subsequently, triethylsilane (1.5 mL, 9.4 mmol) was added dropwise over 20 minutes resulting in an effervescent solution. Once the catalytic hydrogenation was complete, the reaction mixture was filtered over Celite to remove the remaining Pd/C. The solvent was removed by rotary evaporation followed by a gentle stream of air. The dried product was redissolved in chloroform (10 mL), to which 3,4-dibutoxy-3-cyclobutene-1,2-dione (10 μL , 0.5 mmol) and DIPEA (121 μL , 0.9 mmol) were added. Purification of the crude product was performed by flash column chromatography on a C18 silica column with a gradient of 10-90% $\text{CH}_3\text{CN}/\text{H}_2\text{O}$ over 40 minutes. The purified product was concentrated using a rotary evaporator and lyophilized overnight to yield a white solid.

Yield: 39 %, 150 mg. $^1\text{H-NMR}$ (δ_{H} [ppm], CDCl_3 , 400 MHz): 4.77-4.72 (m, 2H), 4.24-4.21 (m, 1H), 3.70-3.54 (m, 42H), 3.48-3.38 (m, 7H), 3.17-3.13 (m, 1H), 1.82-1.75 (m, 2H), 1.64-1.56 (m, 4H), 1.49-1.40 (m, 4H), 1.33-1.29 (m, 16H), 1.00-0.94 (t, 3H). $^{13}\text{C-NMR}$ (δ_{C} [ppm], CDCl_3 , 100 MHz): 189.54, 182.93, 177.36, 172.42, 156.43, 74.30, 73.38, 71.89, 71.85, 71.48, 70.53, 70.02, 66.67, 65.54, 63.80, 59.03, 58.98, 55.22, 54.25, 44.86, 41.05, 36.14, 34.09, 32.29, 32.00, 31.77, 30.66, 29.93, 29.58, 29.44, 29.38, 29.21, 29.10, 28.71, 28.13, 26.71, 26.33, 26.03, 18.63, 18.50, 13.68, 13.58. LC-MS: $t = 7.75$ min, m/z : 824.67 $[\text{M}+\text{H}]^+$

Synthesis of 1b

Compound **6** (150 mg, 0.2 mmol) and DIPEA (5 drops) were added to chloroform (3 mL). Subsequently, 1,7-heptanediamine (41 μ L, 0.3 mmol) was added in 10 μ L aliquots every 2-3 hours to the reaction mixture. After complete addition, the solution was refluxed overnight. Purification of the resulting compound was performed by flash column chromatography on a C18 silica column with a gradient of 30-90% CH₃CN/H₂O over 40 minutes. The collected fractions were combined, concentrated under reduced pressure in a rotary evaporator and lyophilized to yield a white spongy solid.

Yield: 42 %, 62 mg. ¹H-NMR (δ_{H} [ppm], CDCl₃, 600 MHz): 7.77 (br s, 1H), 7.53 (br s, 1H), 4.22 (br s, 1H), 3.77-3.64 (m, 88H), 3.60-3.44 (m, 12H), 3.39 (s, 6H), 1.97-1.55 (m, 10H), 1.41-1.27 (m, 32H). ¹³C-NMR (δ_{C} [ppm], CDCl₃, 150 MHz): 182.80, 181.70, 169.08, 167.22, 72.02, 71.98, 71.67, 71.59, 70.69, 70.65, 70.62, 70.58, 70.56, 70.07, 69.80, 63.89, 62.88, 59.15, 44.84, 43.25, 41.15, 31.32, 30.05, 29.72, 29.65, 29.62, 29.47, 29.41, 26.55, 26.18, 24.82. LC-MS: *t* = 7.47 min, *m/z*: 1630.27 [M+H]⁺



Scheme S3.2. Synthetic route for compounds **2a-b**.

Synthesis of 2a

Compound **1a** (76 mg, 0.05 mmol) was dissolved in dry acetonitrile (5 mL). Pentathiodiphosphorus(V) acid-P,P'-bis(pyridinium betaine) (340 mg, 0.9 mmol) was added to the reaction mixture and stirred overnight at room temperature. The product was purified by reverse phase high-performance liquid chromatography on a C18 column using a gradient of 10-70% CH₃CN/H₂O over 30 minutes. The product was concentrated by rotary evaporation and lyophilized overnight to obtain a yellow solid.

Yield: 89 %, 70.4 mg. ¹H-NMR (δ_H[ppm], CDCl₃, 600 MHz): 8.28 (br s, 2H), 8.42 (br s, 2H), 5.01 (br s, 2H), 4.22-4.19 (m, 4H), 4.12 (m, 8H), 3.67-3.53 (m, 88H), 3.38 (s, 6H), 3.17-3.13 (m, 4H), 1.76-1.63 (m, 12H), 1.52-1.27 (m, 34H). ¹³C-NMR (δ_C[ppm], CDCl₃, 150 MHz): 203.92, 203.51, 170.98, 170.92, 156.57, 72.00, 70.58, 69.83, 63.84, 59.14, 58.55, 54.26, 50.99, 44.25, 43.55, 42.62, 41.20, 41.02, 40.53, 31.36, 31.12, 30.03, 29.88, 29.71, 29.53, 29.36, 29.19, 29.03, 27.71, 27.57, 26.85, 26.76, 26.63, 26.51, 26.24, 25.81, 25.55. LC-MS: t = 8.81 min, m/z: 1780.27 [M+H]⁺

Synthesis of 2b

Compound **1b** (10 mg, 6 μmol) was dissolved in dry acetonitrile (2 mL). Pentathiodiphosphorus(V) acid-P,P'-bis(pyridinium betaine) (100 mg, 0.3 mmol) was added to the reaction mixture and stirred overnight at room temperature. The product was purified by reverse phase high-performance liquid chromatography with a C18 column using a gradient of 10-70% CH₃CN/H₂O over 30 minutes. The product was concentrated by rotary evaporation and lyophilized overnight to obtain compound **4** as a sticky yellow solid.

Yield: 67 %, 6.8 mg. ¹H-NMR (δ_H[ppm], CDCl₃, 600 MHz): 4.16-4.13 (m, 4H), 3.68-3.57 (m, 92H), 3.49-3.45 (m, 4H), 3.40 (s, 6H), 1.75-1.74 (m, 6H), 1.60-1.56 (m, 6H), 1.44-1.28 (m, 30 H). ¹³C-NMR (δ_C[ppm], CDCl₃, 150 MHz): 203.59, 170.96, 170.91, 71.99, 71.92, 71.67, 71.62, 71.44, 70.78, 70.62, 70.59, 70.56, 70.50, 70.47, 70.18, 70.03, 59.18, 44.24, 43.41, 40.54, 31.07,

Chapter 3

29.70, 29.61, 29.55, 29.51, 29.25, 29.07, 27.54, 26.65, 26.51, 26.14, 26.05.

LC-MS: t= 8.80 min, m/z : 1694.40 [M+H]⁺

3.6.4. Fourier transform infrared (FTIR) spectroscopy

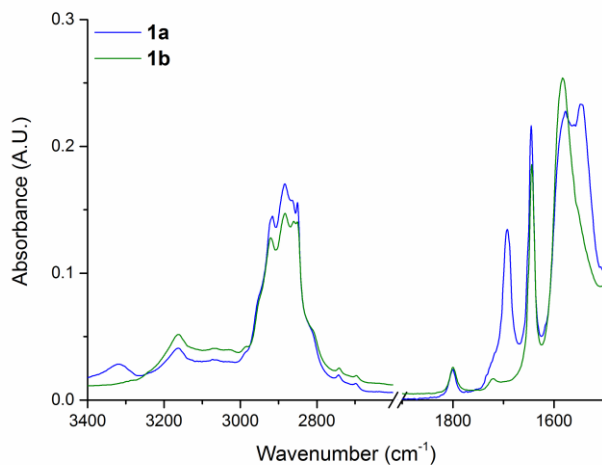


Figure S3.1. Solid FTIR spectra of **1a** and **1b** at room temperature recorded in ATR mode.

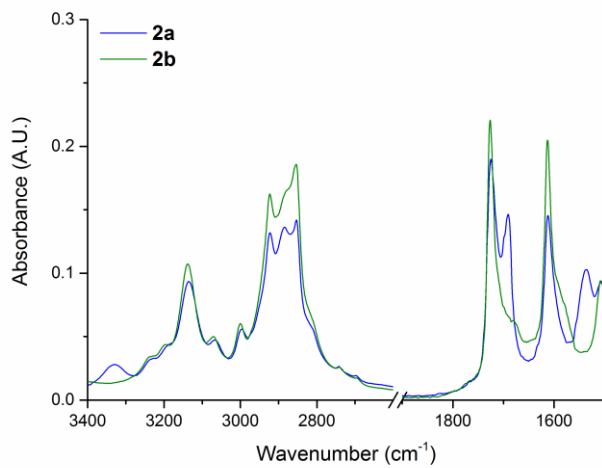


Figure S3.2. Solid FTIR spectra of **2b** and **2b** at room temperature recorded in ATR mode.

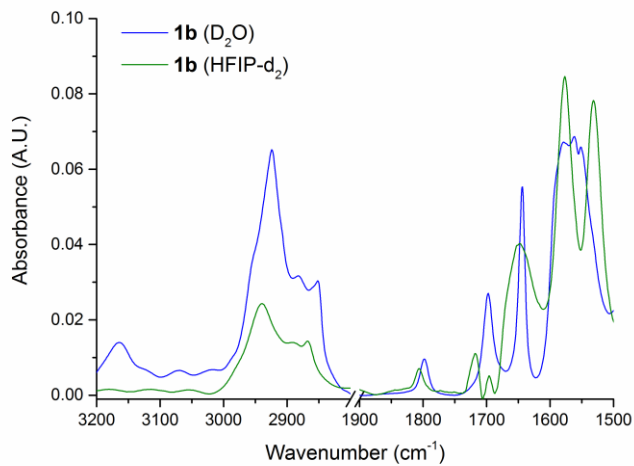


Figure S3.3. FTIR spectra of **1b** in D_2O and HFIP-d_2 .

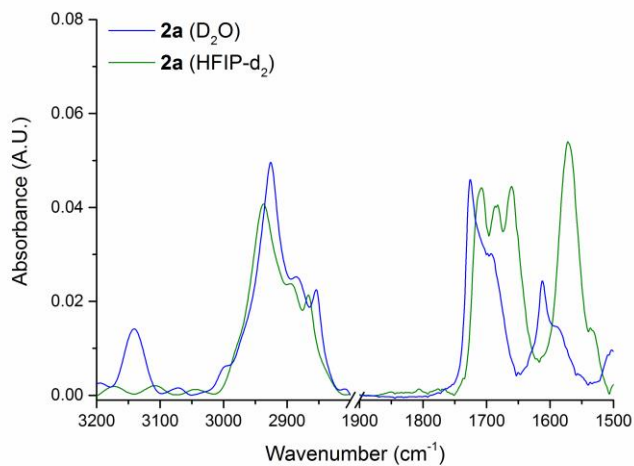


Figure S3.4. FTIR spectra of **2a** in D_2O and HFIP-d_2 .

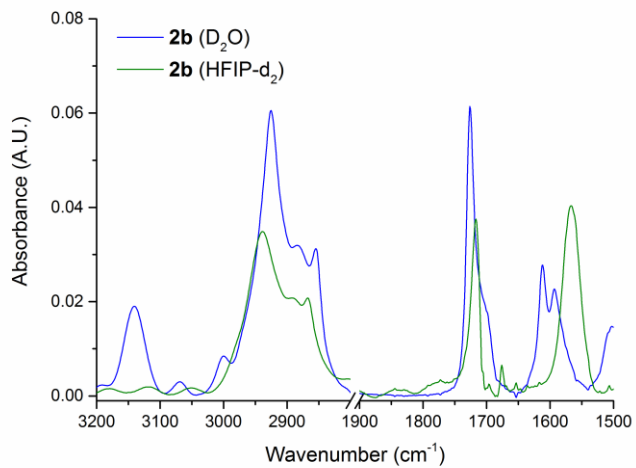


Figure S3.5. FTIR spectra of **2b** in D_2O and HFIP-d_2 .

3.6.5 Cryogenic transmission electron microscopy

Calculation of the persistence length (P_l) and bending rigidity (κ). The cryo-TEM images were converted into text files and imported into the open source software Easyworm developed by Lamour *et al.*¹ We tracked the fiber (**1a**) and rod (**2a**) contour lengths, and then calculated the persistence length and bending rigidity of fibrillar objects above 100 nm for **1a**, and of rod-like objects longer than 20 nm for thionated compounds **2a**. The persistence length was calculated from the mean squared end-to-end distance $\langle R^2 \rangle_{2D}$, which in the worm-like chain (WLC) model for semi-flexible polymers is related to the intercontour length (l) as:

$$\langle R^2 \rangle_{2D} = 4P_l l \left[1 - \frac{2P_l}{l} \left(1 - e^{-\frac{l}{2P_l}} \right) \right]$$

With the P_l , the bending rigidity (κ) of the supramolecular polymers was determined as

$$\kappa = K_b \cdot T \cdot P_l$$

with K_b being the Boltzmann constant, and T the temperature in K.

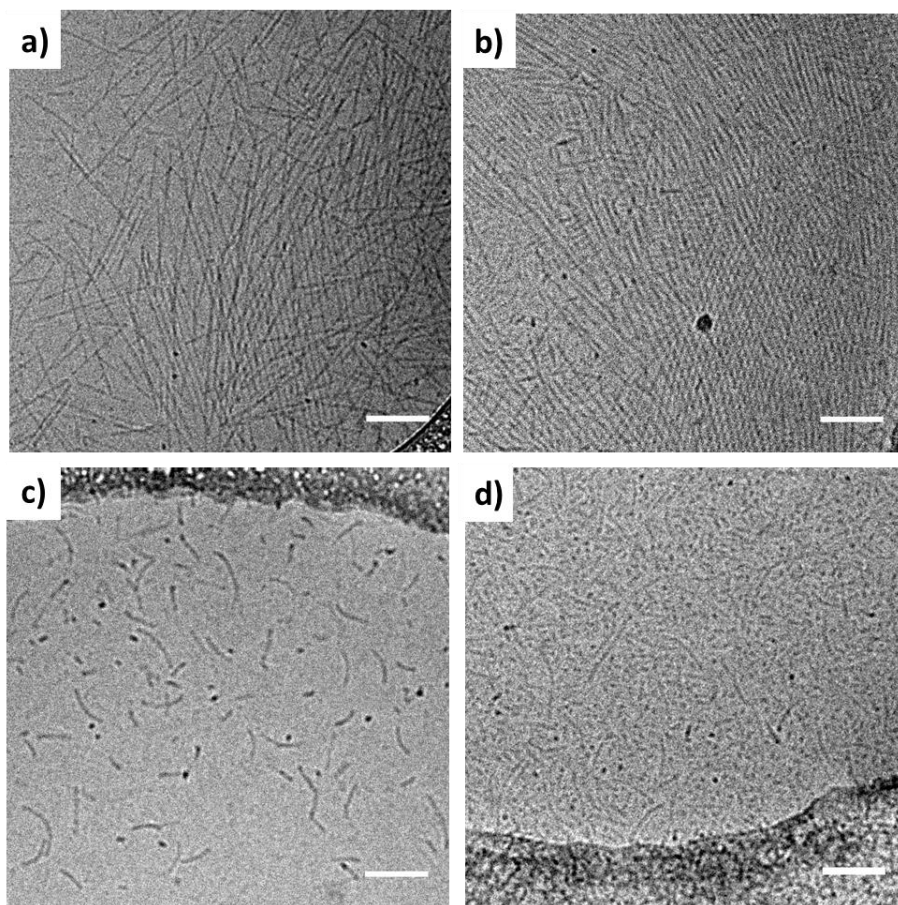


Figure S3.6. CryoTEM images of oxosquaramide-based bolaamphiphiles with carbamate **1a** (a), without carbamate **1b** (b), thiosquaramide-based bolaamphiphiles **2a** with carbamate (c) and without carbamate **2b** (d). Cryo-TEM images of the various squaramide-based monomers were taken at a 10-fold lower concentration (580 μM) compared to an earlier publication.²

Chapter 3

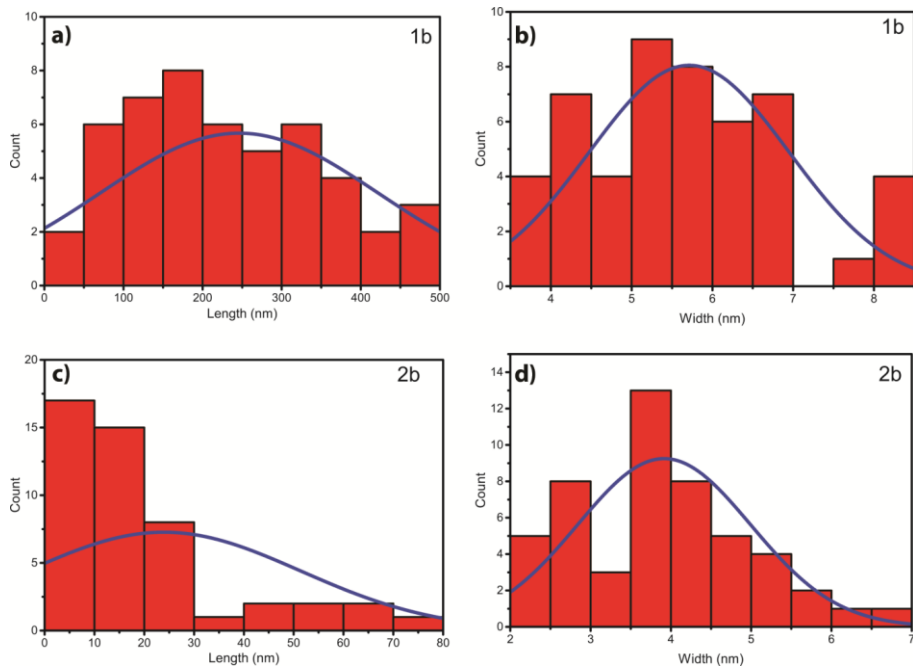


Figure S3.7. Histograms of length and width distributions of **1b** (a, b) and **2b** (c, d) ($N = 50$; average length: 246 ± 176 nm for **1b**, and 24 ± 27 nm for **2b**; average width: 5.7 ± 1.2 nm for **1b**, and 3.9 ± 1.1 nm for **2b**).

3.6.6 Small angle X-ray scattering (SAXS)

The calibration of the beam center and the q -range was achieved by using silver behenate as a standard. The SAXS patterns were brought to an absolute intensity scale using the calibrated detector response function, known sample-to-detector distance, measured incident and transmitted beam intensities, and azimuthally averaged to obtain one dimensional SAXS profiles. The scattering curves of the self-assembled fibers were obtained by subtraction of the scattering contribution of the solvent and quartz cell, by SAXS utilities (<http://www.sztucki.de/SAXSutilities/>). The resulting SAXS profiles were analyzed using the software package SasView (<http://www.sasview.org/>).

SAXS experiments were performed to study the supramolecular polymers constructed from the oxosquaramide and thiosquaramide bolaamphiphiles in water at room temperature. The SAXS profiles of the 4 and 5 mg/mL samples are provided in **Figure S3.8** for the 4 different molecules used in this study. In the low- q regime, the scattering profiles decay with a powerlaw slope of unity for the samples **1a**, **1b** and **2a**. This slope is characteristic for scattering profiles of 1D objects (the length for these structures is beyond the resolution of the experiment ($\sim\pi/q_{\min} = 48$ nm)). Sample **2b** presented a powerlaw slope of 0.72, likely due to the coexistence in solution of two morphologies: rod-like and spherical objects. Upon normalization to 1 mg mL^{-1} , the SAXS profiles taken at 4 and 5 mg mL^{-1} superpose, which means that interfiber interactions can be ignored at these length scales.

The Casassa–Holtzer plot of the data for **1a**, **1b** and **2a** is given in **Figure S3.9**. Similar data treatment was performed for molecule **2b** by using the estimated slope for $I_{cs}(q)$ determination. We extract the cross-sectional mass per unit length, M_L , from the height of the resulting plateau according to

$$\frac{d\Sigma(q)}{d\Omega} = I(q) = \frac{\pi}{q} I_{cs}(q)$$

$$M_L = \frac{I_{cs}(0)}{c\Delta\rho_M^2}$$

with $\Delta\rho_M$ being the electron length density difference per mass, extracted from the fitting curves in SasView.

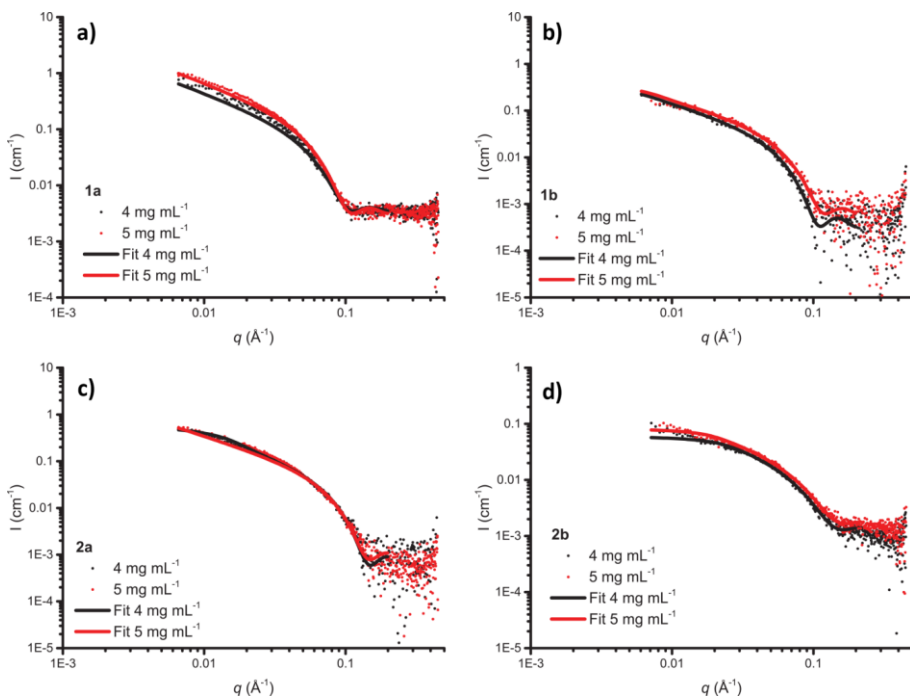


Figure S3.8. SAXS profiles of supramolecular polymers of **1a** (a), **1b** (b), **2a** (c) and **2b** (d), collected at a concentration of 4 and 5 mg mL⁻¹ (the symbols correspond to experimental data (I vs. q) and the lines represent the form factor employed (homogeneous cylinders for **1a** and **1b**, and flexible cylinders for **2a** and **2b**).

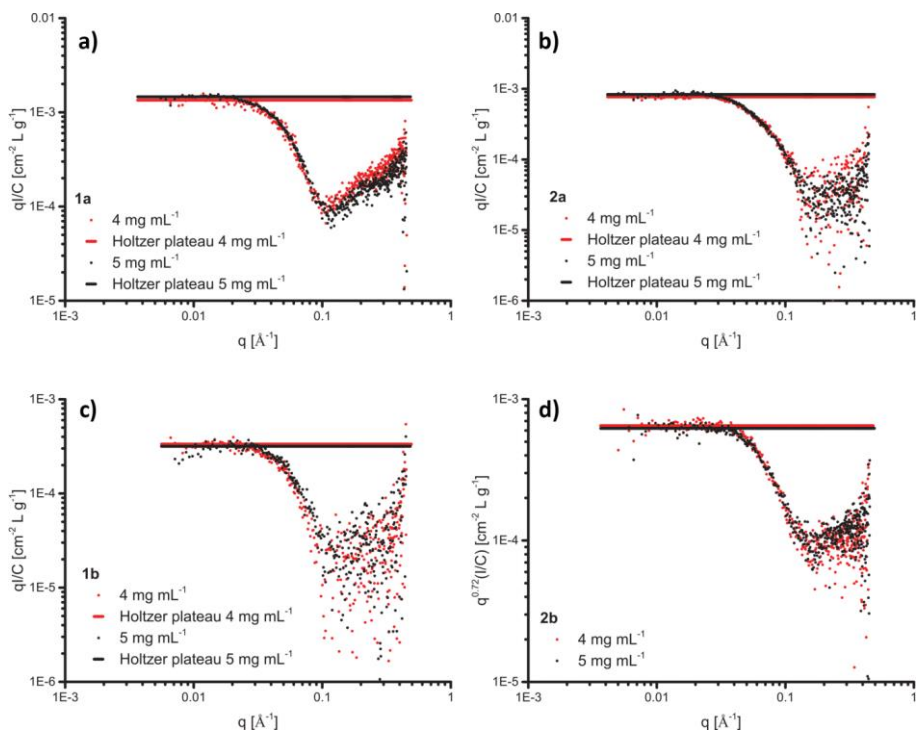


Figure S3.9. Casassa–Holtzer plot of the scattering profiles for monomers **1a**, **1b** and **2a**, and the $I_{CS}(q)$ plateau for **2b**. The plateaus ($0.0066 \leq q \leq 0.0282 \text{ \AA}^{-1}$) are indicated by dashed red and black lines.

Table S3.1. Structural parameters extracted from the SAXS profiles of the oxo- and thiosquaramide-based bolaamphiphiles.

Sample	$\Delta\rho_{\text{cyl}} (\text{Å}^{-2})$	$\Delta\rho_{\text{M}} (\text{cm g}^{-1})$	$I (\text{cm}^{-2} \text{L g}^{-1})$	$I_{\text{cs}} (0) (\text{cm}^{-2})$	$M_{\text{f}} (\text{g nm}^{-1})$	molec/nm	$r_{\text{cs}} (\text{nm})$	Kuhn length (nm)
1a (4 mg/mL)	10.44×10^6	8.91×10^9	1.35×10^5	1.72×10^5	5.41×10^{20}	19	3.4	
1a (5 mg/mL)	10.46×10^6	9.07×10^9	1.46×10^5	2.32×10^5	5.65×10^{20}	20	3.4	
1b (4 mg/mL)	9.94×10^6	4.72×10^9	3.33×10^4	4.25×10^4	4.78×10^{20}	18	3.4	
1b (5 mg/mL)	9.99×10^6	5.12×10^9	3.17×10^4	5.05×10^4	3.86×10^{20}	14	3.2	
2a (4 mg/mL)	10.44×10^6	8.64×10^9	9.45×10^4	1.20×10^5	4.03×10^{20}	14	2.3	4.5
2a (5 mg/mL)	10.50×10^6	9.42×10^9	8.30×10^4	1.32×10^5	2.98×10^{20}	10	2.3	14.1
2b (4 mg/mL)	10.10×10^6	6.03×10^9	6.49×10^4	8.27×10^4	5.68×10^{20}	20	2.3	17.1
2b (5 mg/mL)	10.10×10^6	6.02×10^9	6.21×10^4	9.89×10^4	5.46×10^{20}	19	2.2	21.0

Finally, we model the experimental data using a form factor developed for homogeneous (**1a** and **1b**) and flexible cylinders (**2a** and **2b**) (Figure S3.8). Since all samples are dissolved in water, we fix $\rho_{\text{solvent}} = 9.37 \cdot 10^6 \text{ Å}^{-2}$. From the modeled form factors, we obtain values for the cross-sectional radius of the fibers, r_{cs} , and their electron length density, ρ_{cyl} (see Table S3.1).

3.6.7 UV-Vis spectroscopy

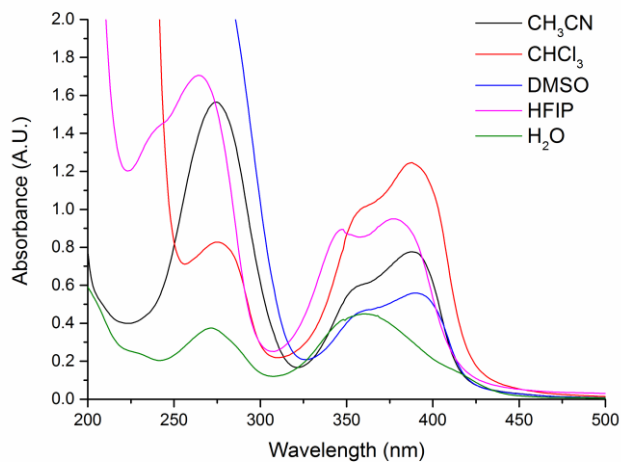


Figure S3.10. UV-Vis spectra of **2a** (30 μM) in various solvents at room temperature.

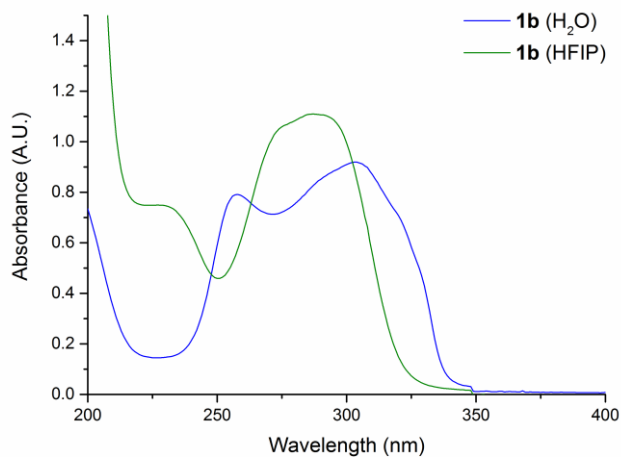


Figure S3.11. UV-Vis spectra of **1b** (30 μM) in water and HFIP.

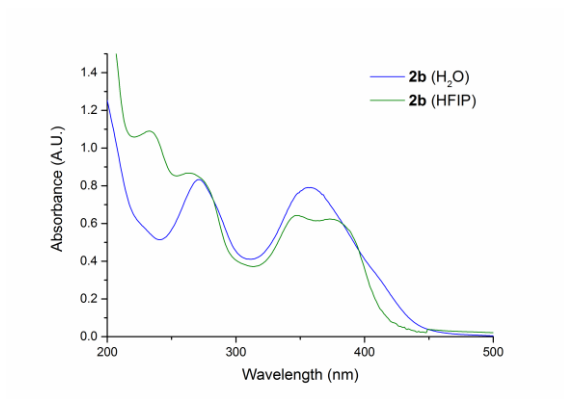


Figure S3.12. UV-Vis spectra of **2b** (30 μM) in water and HFIP.

3.6.8 Comparison of computed “head-to-tail” vs. “stacked” geometries in implicit solvation

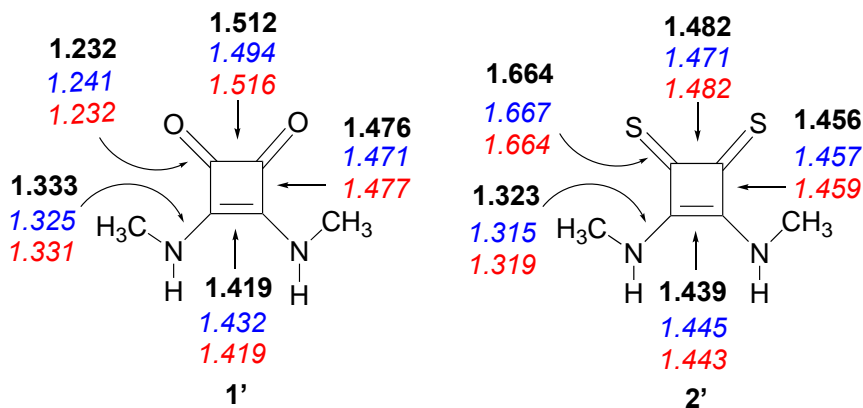


Figure S3.13. Computed geometries in implicit solvation (at $\epsilon = 16.7$) at IEF-PCM-B3LYP-D3/6-31+G(d) for the isolated monomers (bond distances in Å, values in bold font), “head-to-tail” hexamers (values in italics font, in blue), and “stacked” hexamers (values in italics, in red) of **1'** and **2'**. For hexamer structures, the bond distances shown above are based on the average of each monomeric unit.

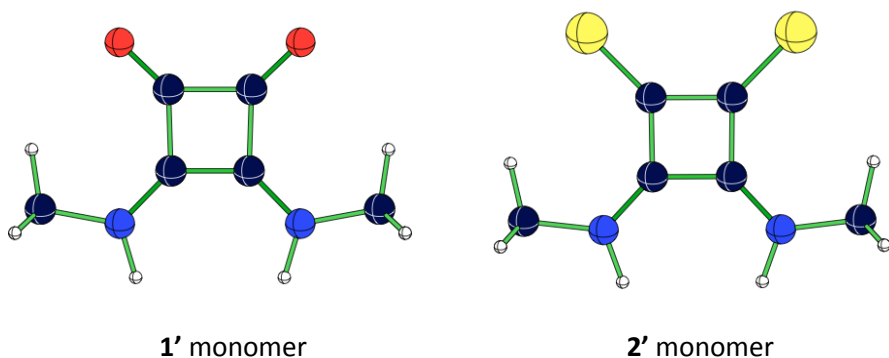


Figure S3.14. Computed structure in implicit solvation (at $\epsilon = 16.7$) at IEF-PCM-B3LYP-D3/6-31+G(d) for the monomers of **1'** and **2'** (see optimized Cartesian coordinates in Table S3.8).

Chapter 3

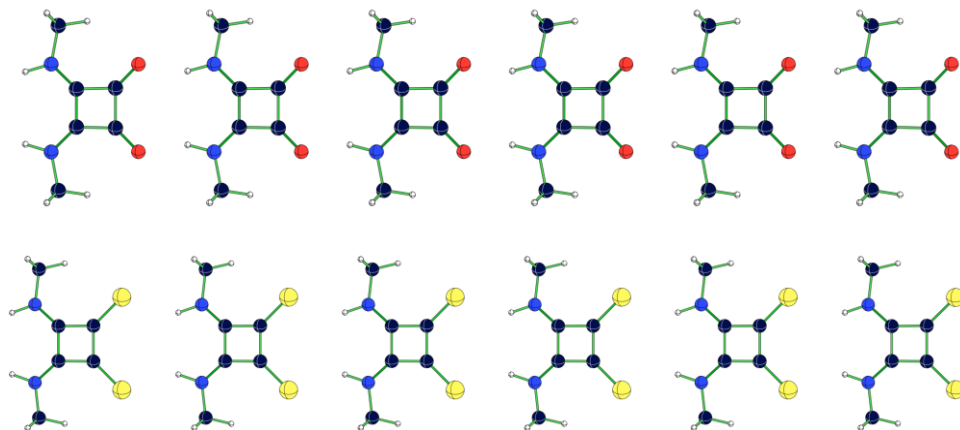


Figure S3.15. Top view of computed structure in implicit solvation (at $\epsilon = 16.7$) at IEF-PCM-B3LYP-D3/6-31+G(d) for the “head-to-tail” hexamers of **1'** (top) and **2'** (bottom) (see optimized Cartesian coordinates in Table S3.8).

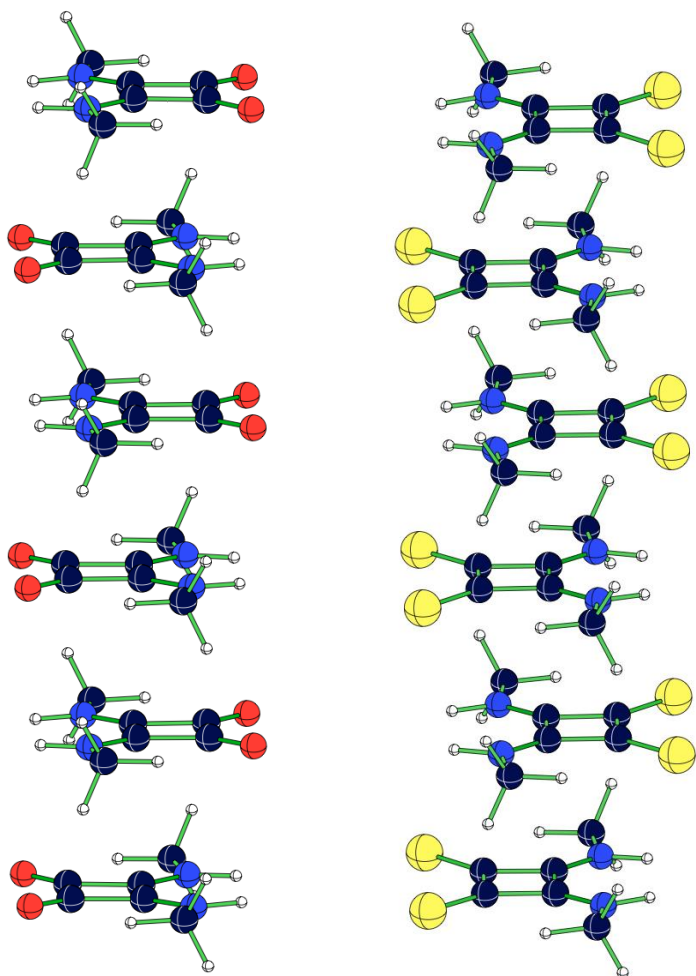


Figure S3.16. Side view of computed structure in implicit solvation (at $\epsilon = 16.7$) at IEF-PCM-B3LYP-D3/6-31+G(d) for the “stacked” hexamers of **1'** (left) and **2'** (right) (see optimized Cartesian coordinates in Supplementary Table 8).

3.6.9 Block-Localized Wave function (BLW) method

Block-Localized Wavefunction (BLW) computations, the most efficient variant of *ab initio* valence bond theory, quantified the π -electron delocalization energies (DE_π) of the isolated N-methyl thiosquaramide monomers (**1'** and **2'**) and of the individual monomer units in the “head-to-tail” and “stacked” hexamers of **1'** and **2'**. The DE_π values for each of the monomer rings were computed by comparing the energy of the fully delocalized wavefunction (ψ_{deloc}) of the monomer to that of its hypothetical π -electron localized wavefunction (ψ_{loc}), in which the expansion of molecular orbitals over basis functions were restricted to a selected subspace in the molecule [$DE_\pi = E(\psi_{\text{deloc}}) - E(\psi_{\text{loc}})$]. For **1'** and **2'**, ψ_{loc} was constructed by partitioning the electrons and basis functions of the molecule into six subspaces (“blocks”); two blocks for the two nitrogen π -lone pairs, two blocks for the C=X π -bonds (X = O or S), one block for the C=C π -bond, and one block for the remaining sigma electrons (see scheme below). Each π -block included two π -electrons (four for the C=S π -bonds) and the p_z , d_{xz} , d_{yz} basis functions belonging to the heavy atoms in the blocks. The computed DE_π values of the isolated **1'** and **2'** monomers were compared to those of the monomer units in the “head-to-tail” and “stacked” hexamers, and the resulting ΔDE_π difference provided a measure of the extra “gain” in π -electron delocalization in **1'** or **2'** upon self-assembly through noncovalent interactions [$\Delta DE_\pi = \Sigma DE_\pi$ (“head-to-tail” or “stacked” monomers) – DE_π (monomer)]. All BLW computations were performed in implicit solvation (at $\epsilon = 8.5$) at the B3LYP/6-31G(d)//IEF-PCM-B3LYP-D3//6-31+G(d) level, employing GAMESS 2013-R1.

Table S3.2. Computed BLW- ΔDE_{π} values (in kcal/mol) for each of the monomer rings in the “head-to-tail” and “stacked” hexamers of **1'** and **2'** in implicit solvation. More negative ΔDE_{π} values indicate greater cyclic π -electron delocalization gain in the monomers upon self-assembly.

Ring	1'		2'	
	“head-to-tail”	“stacked”	“head-to-tail”	“stacked”
A	-14.87	-8.77	-15.15	-12.41
B	-31.06	-17.11	-29.87	-25.58
C	-34.49	-15.73	-33.08	-22.55
D	-34.55	-15.74	-33.13	-22.55
E	-31.82	-17.11	-30.12	-25.58
F	-17.90	-8.77	-16.67	-12.41

3.6.10 Harmonic Oscillator Model of Electron Delocalization (HOMED) index

HOMED is a geometric criterion for evaluating the aromaticity of heterocycles:

$$\text{HOMED} = 1 - \frac{1}{n} \left\{ \alpha_{CC} \sum [R_o(\text{CC}) - R_i(\text{CC})]^2 + \alpha_{CX} \sum [R_o(\text{CX}) - R_i(\text{CX})]^2 \right\} \quad (1)$$

where α_{CC} and α_{CX} are calculated as

$$\alpha_{2i} = 2 \left\{ (R_o - R_s)^2 + (R_o - R_d)^2 \right\}^{-1} \quad \text{for an even number of bonds} \quad (2)$$

$$\alpha_{2i+1} = (2i+1) \left\{ (i+1)(R_o - R_s)^2 + i(R_o - R_d)^2 \right\}^{-1} \quad \text{for an odd number of bonds}$$

R_s (single bond length), R_d (double bond length) and R_o (optimal bond length) are the computed reference bond lengths for CC, CN, CO and CS bonds based on the reference molecules shown on the right. All reference bond lengths and HOMED parameters were computed based on geometries optimized in implicit solvation (at $\epsilon = 16.7$) at IEF-PCM-B3LYP-D3/6-31+G(d) (see Table S3.3).

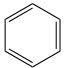
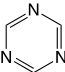
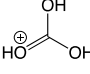
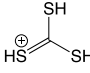
Bond	R_s	R_d	R_o
C-C	<chem>H3C-CH3</chem>	<chem>H2C=CH2</chem>	
C-N	<chem>H3C-NH2</chem>	<chem>H2C=NH</chem>	
C-O	<chem>H3C-OH</chem>	<chem>H2C=O</chem>	
C-S	<chem>H3C-SH</chem>	<chem>H2C=S</chem>	

Table S3.3. Computed parameters for HOMED analysis.

Bond	R_s	R_d	R_o	α_{2i}
CC	1.533 Å	1.336 Å	1.400 Å	91.630
CN	1.446 Å	1.275 Å	1.338 Å	128.070
CO	1.433 Å	1.215 Å	1.285 Å	74.870
CS	1.841 Å	1.624 Å	1.723 Å	84.553

Table S3.4. Computed HOMED values for squaramide units in the “head-to-tail” and “stacked” hexamers of **1'** and **2'** based on geometries optimized in implicit solvation.

Ring	1'		2'	
	“head-to-tail”	“stacked”	“head-to-tail”	“stacked”
A	0.361	0.328	0.447	0.444
B	0.392	0.330	0.454	0.442
C	0.394	0.330	0.454	0.447
D	0.394	0.330	0.455	0.448
E	0.392	0.332	0.455	0.442
F	0.367	0.328	0.456	0.444
Isolated monomer	0.329		0.447	

3.6.11 Nucleus-Independent Chemical Shifts (NICS) analysis

Table S3.5. Computed isotropic NICS values (in ppm) for the “head-to-tail” and “stacked” hexamers of **1'** (computed at 0.6 Å above the ring center of each monomer) and **2'** (computed at 0.8 Å above the ring center of each monomer) in implicit solvation (at $\epsilon = 8.5$) at PW91/IGLOIII//IEF-PCM-B3LYP-D3/6-31+G(d).

Ring	1'		2'	
	“head-to-tail”	“stacked”	“head-to-tail”	“stacked”
A	-6.69	-6.52	-3.65	-3.22
B	-7.07	-7.09	-3.72	-3.64
C	-7.13	-7.88	-3.73	-4.22
D	-7.16	-7.95	-3.75	-4.40
E	-7.19	-7.60	-3.78	-4.56
F	-7.25	-6.95	-3.85	-3.90
Isolated Monomer	-6.95 ppm		-3.73 ppm	

3.6.12 Computed IR frequencies and intensities

Table S3.6. Computed infrared (IR) stretching frequencies (values in cm^{-1}) for the monomer, “head-to-tail” hexamer, and “stacked” hexamer of **1'** in implicit solvation (at $\epsilon = 8.5$) at IEF-PCM-B3LYP-D3/6-31+G(d).

Mode	monomer	head-to-tail	stacked
C=O sym. stretching	1654	1547-1667	1547-1652
C=O antisym. stretching	1580	1579-1698	1581-1718
Ring breathing	1851	1847-1859	1851-1866
N–H sym. stretching	3592	3320-3369	3585-3589
N–H antisym. stretching	3577	3307-3573	3570-3573

Table S3.7. Computed infrared (IR) stretching frequencies (values in cm^{-1}) and intensities (italicized, in parenthesis) for the monomer, “head-to-tail” hexamer, and “stacked” hexamer of **2'** in implicit solvation (at $\epsilon = 8.5$) at IEF-PCM-B3LYP-D3/6-31+G(d).

Mode	monomer	head-to-tail	stacked
C=S sym. stretching	1324	1226-1330	1230-1330
C=S antisym. stretching	1164	1154-1272	1174-1274
Ring breathing	1757	1764-1774	1761-1774
N–H sym. stretching	3579	3349-3577	3574-3576
N–H antisym. stretching	3564	3342-3561	3561-3564

3.6.13 Cartesian coordinates of optimized geometries

Table S3.8. Optimized Cartesian coordinates (in Å) and computed total electronic energies for the isolated monomers (constrained to C_{2v}), “head-to-tail” hexamers (constrained to C_{2v}), and “stacked” hexamers (constrained to C_s) of **1'** and **2'** in implicit solvation (at $\epsilon = 16.7$) at IEF-PCM-B3LYP-D3/6-31+G(d).

1' monomer (C_{2v})

	X	Y	Z
C	-1.46569	-1.47504	0.00000
C	-0.04627	-1.47504	0.00000
C	-1.51196	0.00000	0.00000
C	0.00000	0.00000	0.00000
N	-2.39609	-2.43032	0.00000
N	0.88413	-2.43032	0.00000
C	-3.83615	-2.16669	0.00000
C	2.32419	-2.16669	0.00000
O	-2.40268	0.85105	0.00000
O	0.89072	0.85105	0.00000
H	-4.29981	-2.60020	-0.89210
H	-4.29981	-2.60020	0.89210
H	2.78785	-2.60020	-0.89210
H	2.78785	-2.60020	0.89210
H	-3.99798	-1.08827	0.00000
H	2.48602	-1.08827	0.00000
H	0.59429	-3.40114	0.00000
H	-2.10624	-3.40114	0.00000

Total electronic energy = -493.4185755 a.u.

1' “head-to-tail” hexamer (C_{2v})

	X	Y	Z
C	0.25080	0.74470	0.00000
C	0.25080	-0.74470	0.00000
O	1.11927	1.63393	0.00000
O	1.11927	-1.63393	0.00000
C	-1.21865	0.71732	0.00000
C	-1.21865	-0.71732	0.00000
N	-2.16569	1.64074	0.00000

Chapter 3

N	-2.16569	-1.64074	0.00000
H	-3.16100	1.38125	0.00000
H	-3.16100	-1.38125	0.00000
C	-1.88891	3.07761	0.00000
C	-1.88891	-3.07761	0.00000
H	-0.81078	3.24296	0.00000
H	-0.81078	-3.24296	0.00000
H	-2.32661	3.54120	-0.89018
H	-2.32661	-3.54120	0.89018
H	-2.32661	-3.54120	-0.89018
H	-2.32661	3.54120	0.89018
N	-14.38430	-1.64113	0.00000
N	-14.38430	1.64113	0.00000
C	-13.43725	-0.71697	0.00000
C	-13.43725	0.71697	0.00000
C	-11.96780	-0.74503	0.00000
C	-11.96780	0.74503	0.00000
O	-11.09995	-1.63406	0.00000
O	-11.09995	1.63406	0.00000
C	-14.10864	-3.07842	0.00000
C	-14.10864	3.07842	0.00000
N	-8.27422	-1.64078	0.00000
N	-8.27422	1.64078	0.00000
C	-7.32723	-0.71732	0.00000
C	-7.32723	0.71732	0.00000
C	-5.85782	-0.74465	0.00000
C	-5.85782	0.74465	0.00000
O	-4.98933	-1.63387	0.00000
O	-4.98933	1.63387	0.00000
C	-7.99759	-3.07771	0.00000
C	-7.99759	3.07771	0.00000
C	-19.56333	0.71355	0.00000
C	-19.56333	-0.71355	0.00000
C	-18.09328	-0.74838	0.00000
C	-18.09328	0.74838	0.00000
O	-17.23072	1.63572	0.00000

O	-17.23072	-1.63572	0.00000
N	-20.51151	1.64342	0.00000
N	-20.51151	-1.64342	0.00000
H	-21.48361	1.35617	0.00000
H	-21.48361	-1.35617	0.00000
C	-20.24356	-3.08403	0.00000
C	-20.24356	3.08403	0.00000
H	-19.16501	-3.24387	0.00000
H	-19.16501	3.24387	0.00000
H	-20.67776	-3.54529	0.89235
H	-20.67776	3.54529	-0.89235
H	-20.67776	3.54529	0.89235
H	-20.67776	-3.54529	-0.89235
H	-15.37684	1.37966	0.00000
H	-15.37684	-1.37966	0.00000
H	-13.03054	-3.24357	0.00000
H	-13.03054	3.24357	0.00000
H	-14.54617	-3.54165	0.89038
H	-14.54617	3.54165	-0.89038
H	-14.54617	3.54165	0.89038
H	-14.54617	-3.54165	-0.89038
H	-9.26926	1.38108	0.00000
H	-9.26926	-1.38108	0.00000
H	-6.91948	-3.24309	0.00000
H	-6.91948	3.24309	0.00000
H	-8.43532	-3.54121	0.89020
H	-8.43532	3.54121	-0.89020
H	-8.43532	3.54121	0.89020
H	-8.43532	-3.54121	-0.89020
C	4.89249	0.71694	0.00000
C	4.89249	-0.71694	0.00000
C	6.36237	-0.74536	0.00000
C	6.36237	0.74536	0.00000
O	7.23010	1.63444	0.00000
O	7.23010	-1.63444	0.00000
N	3.94482	1.64052	0.00000

Chapter 3

N	3.94482	-1.64052	0.00000
H	2.94979	1.38082	0.00000
H	2.94979	-1.38082	0.00000
C	4.22149	-3.07729	0.00000
C	4.22149	3.07729	0.00000
H	5.29964	-3.24258	0.00000
H	5.29964	3.24258	0.00000
H	3.78400	-3.54122	0.89017
H	3.78400	3.54122	-0.89017
H	3.78400	3.54122	0.89017
H	3.78400	-3.54122	-0.89017
C	11.03011	0.71326	0.00000
C	11.03011	-0.71326	0.00000
C	12.50424	-0.75246	0.00000
C	12.50424	0.75246	0.00000
O	13.36200	1.64390	0.00000
O	13.36200	-1.64390	0.00000
N	10.07537	1.63700	0.00000
N	10.07537	-1.63700	0.00000
H	9.08340	1.37341	0.00000
H	9.08340	-1.37341	0.00000
C	10.34712	-3.07361	0.00000
C	10.34712	3.07361	0.00000
H	11.42509	-3.24086	0.00000
H	11.42509	3.24086	0.00000
H	9.91023	-3.53949	0.89005
H	9.91023	3.53949	-0.89005
H	9.91023	3.53949	0.89005
H	9.91023	-3.53949	-0.89005

Total electronic energy = -2960.6149774a.u.

1' "stacked" hexamer (C_s)

	X	Y	Z
C	-6.40975	1.79408	-0.70977
C	-6.40975	1.79408	0.70977
C	-5.83035	3.15135	-0.75734

C	-5.83035	3.15135	0.75734
N	-6.76142	0.90141	-1.63391
N	-6.76142	0.90141	1.63391
C	-6.63408	1.11828	-3.07487
C	-6.63408	1.11828	3.07487
O	-5.47877	3.92455	-1.64922
O	-5.47877	3.92455	1.64922
H	-7.10092	-0.00654	1.33841
H	-7.10092	-0.00654	-1.33841
H	-5.94373	0.38497	-3.50343
H	-5.94373	0.38497	3.50343
H	-6.24839	2.12322	-3.24862
H	-6.24839	2.12322	3.24862
H	-7.61097	1.01844	-3.55844
H	-7.61097	1.01844	3.55844
C	-3.28468	0.69424	0.70972
C	-3.28468	0.69424	-0.70972
C	-3.84072	-0.67277	0.75854
C	-3.84072	-0.67277	-0.75854
N	-2.91597	1.58607	1.62551
N	-2.91597	1.58607	-1.62551
C	-3.00055	1.37233	3.06853
C	-3.00055	1.37233	-3.06853
O	-4.15977	-1.45820	1.65214
O	-4.15977	-1.45820	-1.65214
H	-2.56201	2.48573	-1.32157
H	-2.56201	2.48573	1.32157
H	-2.00624	1.46242	3.51648
H	-2.00624	1.46242	-3.51648
H	-3.39227	0.37234	3.25575
H	-3.39227	0.37234	-3.25575
H	-3.66821	2.11421	3.51718
H	-3.66821	2.11421	-3.51718
C	-0.29946	-0.65756	-0.70946
C	-0.29946	-0.65756	0.70946
C	0.26239	0.70717	-0.75890

Chapter 3

C	0.26239	0.70717	0.75890
N	-0.66649	-1.55032	-1.62550
N	-0.66649	-1.55032	1.62550
C	-0.57420	-1.33935	-3.06847
C	-0.57420	-1.33935	3.06847
O	0.58611	1.48972	-1.65284
O	0.58611	1.48972	1.65284
H	-1.03150	-2.44550	1.32144
H	-1.03150	-2.44550	-1.32144
H	0.09077	-2.08621	-3.51305
H	0.09077	-2.08621	3.51305
H	-0.17506	-0.34222	-3.25544
H	-0.17506	-0.34222	3.25544
H	-1.56676	-1.42401	-3.52131
H	-1.56676	-1.42401	3.52131
C	2.78162	-1.77984	0.70946
C	2.78162	-1.77984	-0.70946
C	2.21977	-3.14456	0.75890
C	2.21977	-3.14456	-0.75890
N	3.14864	-0.88707	1.62550
N	3.14864	-0.88707	-1.62550
C	3.05635	-1.09804	3.06847
C	3.05635	-1.09804	-3.06847
O	1.89604	-3.92711	1.65284
O	1.89604	-3.92711	-1.65284
H	3.51366	0.00811	-1.32144
H	3.51366	0.00811	1.32144
H	4.04891	-1.01338	3.52131
H	4.04891	-1.01338	-3.52131
H	2.65722	-2.09517	3.25545
H	2.65722	-2.09517	-3.25545
H	2.39138	-0.35118	3.51305
H	2.39138	-0.35118	-3.51305
C	5.76683	-3.13163	-0.70972
C	5.76683	-3.13163	0.70972
C	6.32287	-1.76462	-0.75854

C	6.32287	-1.76462	0.75854
N	5.39813	-4.02346	-1.62551
N	5.39813	-4.02346	1.62551
C	5.48271	-3.80972	-3.06853
C	5.48271	-3.80972	3.06853
O	6.64192	-0.97919	-1.65214
O	6.64192	-0.97919	1.65214
H	5.04417	-4.92313	1.32157
H	5.04417	-4.92313	-1.32157
H	6.15038	-4.55160	-3.51717
H	6.15038	-4.55160	3.51717
H	5.87443	-2.80973	-3.25575
H	5.87443	-2.80973	3.25575
H	4.48840	-3.89982	-3.51648
H	4.48840	-3.89982	3.51648
C	8.89191	-4.23146	0.70977
C	8.89191	-4.23146	-0.70977
C	8.31251	-5.58873	0.75734
C	8.31251	-5.58873	-0.75734
N	9.24359	-3.33880	1.63391
N	9.24359	-3.33880	-1.63391
C	9.11624	-3.55566	3.07487
C	9.11624	-3.55566	-3.07487
O	7.96093	-6.36193	1.64922
O	7.96093	-6.36193	-1.64922
H	9.58310	-2.43085	-1.33841
H	9.58310	-2.43085	1.33841
H	10.09313	-3.45582	3.55845
H	10.09313	-3.45582	-3.55845
H	8.73055	-4.56060	3.24863
H	8.73055	-4.56060	-3.24863
H	8.42588	-2.82236	3.50342
H	8.42588	-2.82236	-3.50342

Total electronic energy = -2960.5861726 a.u.

2' monomer (C_{2v})

Chapter 3

	X	Y	Z
C	-0.02112	-1.43894	0.00000
C	0.00000	0.00000	0.00000
C	1.43442	-1.48168	0.00000
C	1.45617	0.00000	0.00000
N	-1.00832	-2.31907	0.00000
N	-0.96093	0.90873	0.00000
C	-0.86004	-3.77702	0.00000
C	-0.76992	2.36170	0.00000
S	2.60713	-2.66232	0.00000
S	2.66303	1.14571	0.00000
H	-1.92125	0.58154	0.00000
H	-1.95861	-1.96383	0.00000
H	-1.33599	-4.19361	0.89268
H	-1.23344	2.79208	0.89268
H	0.19996	-4.02789	0.00000
H	0.29699	2.58135	0.00000
H	-1.33599	-4.19361	-0.89268
H	-1.23344	2.79208	-0.89268

Total electronic energy = -1139.3393076 a.u.

2' "head-to-tail" hexamer (C_{2v})

	X	Y	Z
C	0.71525	0.73462	0.00000
C	0.71525	-0.73462	0.00000
S	1.89509	1.91855	0.00000
S	1.89509	-1.91855	0.00000
C	-0.74136	0.72364	0.00000
C	-0.74136	-0.72364	0.00000
N	-1.71175	1.60931	0.00000
N	-1.71175	-1.60931	0.00000
H	-2.68530	1.28371	0.00000
H	-2.68530	-1.28371	0.00000
C	-1.54716	3.06459	0.00000
C	-1.54716	-3.06459	0.00000
H	-0.48689	3.31356	0.00000

H	-0.48689	-3.31356	0.00000
H	-2.02482	3.48221	-0.89124
H	-2.02482	-3.48221	0.89124
H	-2.02482	-3.48221	-0.89124
H	-2.02482	3.48221	0.89124
N	-15.54516	-1.60857	0.00000
N	-15.54516	1.60857	0.00000
C	-14.57384	-0.72333	0.00000
C	-14.57384	0.72333	0.00000
C	-13.11739	-0.73493	0.00000
C	-13.11739	0.73493	0.00000
S	-11.93824	-1.91883	0.00000
S	-11.93824	1.91883	0.00000
C	-15.38219	-3.06409	0.00000
C	-15.38219	3.06409	0.00000
N	-8.62763	-1.60928	0.00000
N	-8.62763	1.60928	0.00000
C	-7.65722	-0.72363	0.00000
C	-7.65722	0.72363	0.00000
C	-6.20062	-0.73462	0.00000
C	-6.20062	0.73462	0.00000
S	-5.02087	-1.91860	0.00000
S	-5.02087	1.91860	0.00000
C	-8.46314	-3.06459	0.00000
C	-8.46314	3.06459	0.00000
C	-21.50091	0.72143	0.00000
C	-21.50091	-0.72143	0.00000
C	-20.04544	-0.73741	0.00000
C	-20.04544	0.73741	0.00000
S	-18.86877	1.91731	0.00000
S	-18.86877	-1.91731	0.00000
N	-22.47165	1.61457	0.00000
N	-22.47165	-1.61457	0.00000
H	-23.42735	1.27299	0.00000
H	-23.42735	-1.27299	0.00000
C	-22.30583	-3.07152	0.00000

Chapter 3

C	-22.30583	3.07152	0.00000
H	-21.24375	-3.31196	0.00000
H	-21.24375	3.31196	0.00000
H	-22.77837	-3.49091	0.89278
H	-22.77837	3.49091	-0.89278
H	-22.77837	3.49091	0.89278
H	-22.77837	-3.49091	-0.89278
H	-16.51678	1.28026	0.00000
H	-16.51678	-1.28026	0.00000
H	-14.32203	-3.31355	0.00000
H	-14.32203	3.31355	0.00000
H	-15.85973	-3.48149	0.89139
H	-15.85973	3.48149	-0.89139
H	-15.85973	3.48149	0.89139
H	-15.85973	-3.48149	-0.89139
H	-9.60103	1.28348	0.00000
H	-9.60103	-1.28348	0.00000
H	-7.40286	-3.31356	0.00000
H	-7.40286	3.31356	0.00000
H	-8.94077	-3.48219	0.89125
H	-8.94077	3.48219	-0.89125
H	-8.94077	3.48219	0.89125
H	-8.94077	-3.48219	-0.89125
C	6.17620	0.72346	0.00000
C	6.17620	-0.72346	0.00000
C	7.63282	-0.73494	0.00000
C	7.63282	0.73494	0.00000
S	8.81331	1.91790	0.00000
S	8.81331	-1.91790	0.00000
N	5.20546	1.60920	0.00000
N	5.20546	-1.60920	0.00000
H	4.23209	1.28344	0.00000
H	4.23209	-1.28344	0.00000
C	5.37013	-3.06440	0.00000
C	5.37013	3.06440	0.00000
H	6.43049	-3.31311	0.00000

H	6.43049	3.31311	0.00000
H	4.89264	-3.48228	0.89124
H	4.89264	3.48228	-0.89124
H	4.89264	3.48228	0.89124
H	4.89264	-3.48228	-0.89124
C	13.11343	0.72168	0.00000
C	13.11343	-0.72168	0.00000
C	14.57030	-0.73835	0.00000
C	14.57030	0.73835	0.00000
S	15.76263	1.90651	0.00000
S	15.76263	-1.90651	0.00000
N	12.13866	1.60775	0.00000
N	12.13866	-1.60775	0.00000
H	11.16726	1.28006	0.00000
H	11.16726	-1.28006	0.00000
C	12.30442	-3.06206	0.00000
C	12.30442	3.06206	0.00000
H	13.36586	-3.30748	0.00000
H	13.36586	3.30748	0.00000
H	11.82879	-3.48289	0.89119
H	11.82879	3.48289	-0.89119
H	11.82879	3.48289	0.89119
H	11.82879	-3.48289	-0.89119

Total electronic energy = -6836.1167066 a.u.

2' "stacked" hexamer (C_s)

	X	Y	Z
C	0.10182	-0.75181	-0.72066
C	0.10182	-0.75181	0.72066
C	-0.44249	0.60065	-0.74122
C	-0.44249	0.60065	0.74122
N	0.48305	-1.64773	-1.61282
N	0.48305	-1.64773	1.61282
C	0.44278	-1.48739	-3.06826
C	0.44278	-1.48739	3.06826
S	-0.86016	1.71484	-1.90389

Chapter 3

S	-0.86016	1.71484	1.90389
H	0.88599	-2.51438	1.27107
H	0.88599	-2.51438	-1.27107
H	1.46260	-1.53409	-3.46210
H	1.46260	-1.53409	3.46210
H	-0.00493	-0.52422	-3.30960
H	-0.00493	-0.52422	3.30960
H	-0.15524	-2.29180	-3.50580
H	-0.15524	-2.29180	3.50580
C	3.13322	0.63802	0.72178
C	3.13322	0.63802	-0.72178
C	3.69382	-0.70945	0.74110
C	3.69382	-0.70945	-0.74110
N	2.76238	1.53746	1.61066
N	2.76238	1.53746	-1.61066
C	2.82148	1.39468	3.06636
C	2.82148	1.39468	-3.06636
S	4.14999	-1.80696	1.90578
S	4.14999	-1.80696	-1.90578
H	2.38949	2.41712	-1.26732
H	2.38949	2.41712	1.26732
H	3.45510	2.18729	3.47446
H	3.45510	2.18729	-3.47446
H	3.23884	0.41974	3.31390
H	3.23884	0.41974	-3.31390
H	1.81002	1.48263	3.47312
H	1.81002	1.48263	-3.47312
C	6.20596	1.80764	-0.72147
C	6.20596	1.80764	0.72147
C	5.64816	3.15627	-0.74162
C	5.64816	3.15627	0.74162
N	6.57733	0.90775	-1.61049
N	6.57733	0.90775	1.61049
C	6.52313	1.05203	-3.06620
C	6.52313	1.05203	3.06620
S	5.19399	4.25330	-1.90642

S	5.19399	4.25330	1.90642
H	6.94180	0.02484	1.26665
H	6.94180	0.02484	-1.26665
H	7.53575	0.96337	-3.47035
H	7.53575	0.96337	3.47035
H	6.10787	2.02780	-3.31415
H	6.10787	2.02780	3.31415
H	5.89005	0.26066	-3.47750
H	5.89005	0.26066	3.47750
C	9.21057	3.18894	0.72147
C	9.21057	3.18894	-0.72147
C	9.76835	1.84030	0.74162
C	9.76835	1.84030	-0.74162
N	8.83920	4.08884	1.61049
N	8.83920	4.08884	-1.61049
C	8.89340	3.94455	3.06619
C	8.89340	3.94455	-3.06619
S	10.22251	0.74326	1.90641
S	10.22251	0.74326	-1.90641
H	8.47474	4.97174	-1.26664
H	8.47474	4.97174	1.26664
H	9.52650	4.73592	3.47750
H	9.52650	4.73592	-3.47750
H	9.30864	2.96878	3.31415
H	9.30864	2.96878	-3.31415
H	7.88079	4.03324	3.47035
H	7.88079	4.03324	-3.47035
C	12.28335	4.35847	-0.72178
C	12.28335	4.35847	0.72178
C	11.72280	5.70596	-0.74110
C	11.72280	5.70596	0.74110
N	12.65416	3.45901	-1.61066
N	12.65416	3.45901	1.61066
C	12.59506	3.60179	-3.06636
C	12.59506	3.60179	3.06636
S	11.26665	6.80348	-1.90578

Chapter 3

S	11.26665	6.80348	1.90578
H	13.02701	2.57934	1.26732
H	13.02701	2.57934	-1.26732
H	13.60652	3.51381	-3.47312
H	13.60652	3.51381	3.47312
H	12.17773	4.57675	-3.31390
H	12.17773	4.57675	3.31390
H	11.96141	2.80921	-3.47446
H	11.96141	2.80921	3.47446
C	15.31479	5.74819	0.72066
C	15.31479	5.74819	-0.72066
C	15.85905	4.39571	0.74122
C	15.85905	4.39571	-0.74122
N	14.93359	6.64413	1.61282
N	14.93359	6.64413	-1.61282
C	14.97385	6.48379	3.06826
C	14.97385	6.48379	-3.06826
S	16.27669	3.28151	1.90389
S	16.27669	3.28151	-1.90389
H	14.53068	7.51079	-1.27107
H	14.53068	7.51079	1.27107
H	15.57189	7.28817	3.50581
H	15.57189	7.28817	-3.50581
H	15.42152	5.52060	3.30960
H	15.42152	5.52060	-3.30960
H	13.95403	6.53052	3.46209
H	13.95403	6.53052	-3.46209

Total electronic energy = -6836.139497a.u.

Table S3.9. Optimized Cartesian coordinates (in Å) and computed total electronic energies for the isolated monomers (constrained to C_{2v}), “head-to-tail” hexamers (constrained to C_{2v}), and “stacked” hexamers (constrained to C_s) of **1'** and **2'** at ω B97X-D/6-311+G(d,p) in the gas-phase.

1' monomer (C_{2v})

	X	Y	Z
C	0.97683	-0.98889	0.00000
C	0.00000	0.00000	0.00000

C	2.07670	0.00000	0.00000
C	1.00230	1.08766	0.00000
N	0.95696	-2.33029	0.00000
N	-1.34154	-0.00342	0.00000
C	2.16439	-3.14273	0.00000
C	-2.13911	1.21389	0.00000
O	3.27969	-0.06223	0.00000
O	0.95484	2.29132	0.00000
H	2.20638	-3.77483	0.89068
H	2.20638	-3.77483	-0.89068
H	-2.77066	1.26363	0.89068
H	-2.77066	1.26363	-0.89068
H	3.02967	-2.48088	0.00000
H	-1.46670	2.07098	0.00000
H	-1.82866	-0.88377	0.00000
H	0.07069	-2.80657	0.00000

Total electronic energy = -493.3397188 a.u.

ZPE = 0.140953 a.u.

NIm = 2 (65.65 icm^{-1} , 39.67 icm^{-1})

1' "head-to-tail" hexamer (C_{2v})

	X	Y	Z
C	0.22323	0.74547	0.00000
C	0.22323	-0.74547	0.00000
O	1.07506	1.62327	0.00000
O	1.07506	-1.62327	0.00000
C	-1.23989	0.70836	0.00000
C	-1.23989	-0.70836	0.00000
N	-2.18175	1.63633	0.00000
N	-2.18175	-1.63633	0.00000
H	-3.17226	1.38688	0.00000
H	-3.17226	-1.38688	0.00000
C	-1.88313	3.05988	0.00000
C	-1.88313	-3.05988	0.00000
H	-0.80349	3.20525	0.00000
H	-0.80349	-3.20525	0.00000

Chapter 3

H	-2.30926	3.53340	-0.88752
H	-2.30926	-3.53340	0.88752
H	-2.30926	-3.53340	-0.88752
H	-2.30926	3.53340	0.88752
N	-14.37701	-1.63812	0.00000
N	-14.37701	1.63812	0.00000
C	-13.43530	-0.70730	0.00000
C	-13.43530	0.70730	0.00000
C	-11.97178	-0.74643	0.00000
C	-11.97178	0.74643	0.00000
O	-11.12124	-1.62303	0.00000
O	-11.12124	1.62303	0.00000
C	-14.07865	-3.06282	0.00000
C	-14.07865	3.06282	0.00000
N	-8.27429	-1.63677	0.00000
N	-8.27429	1.63677	0.00000
C	-7.33285	-0.70847	0.00000
C	-7.33285	0.70847	0.00000
C	-5.87000	-0.74516	0.00000
C	-5.87000	0.74516	0.00000
O	-5.01734	-1.62230	0.00000
O	-5.01734	1.62230	0.00000
C	-7.97606	-3.06079	0.00000
C	-7.97606	3.06079	0.00000
C	-19.58365	0.70243	0.00000
C	-19.58365	-0.70243	0.00000
C	-18.11691	-0.75176	0.00000
C	-18.11691	0.75176	0.00000
O	-17.27488	1.62692	0.00000
O	-17.27488	-1.62692	0.00000
N	-20.53190	1.63712	0.00000
N	-20.53190	-1.63712	0.00000
H	-21.49827	1.35379	0.00000
H	-21.49827	-1.35379	0.00000
C	-20.24768	-3.06779	0.00000
C	-20.24768	3.06779	0.00000

H	-19.16815	-3.21075	0.00000
H	-19.16815	3.21075	0.00000
H	-20.66709	-3.53941	0.89085
H	-20.66709	3.53941	-0.89085
H	-20.66709	3.53941	0.89085
H	-20.66709	-3.53941	-0.89085
H	-15.36206	1.38473	0.00000
H	-15.36206	-1.38473	0.00000
H	-12.99891	-3.20609	0.00000
H	-12.99891	3.20609	0.00000
H	-14.50212	-3.53671	0.88834
H	-14.50212	3.53671	-0.88834
H	-14.50212	3.53671	0.88834
H	-14.50212	-3.53671	-0.88834
H	-9.26365	1.38642	0.00000
H	-9.26365	-1.38642	0.00000
H	-6.89647	-3.20609	0.00000
H	-6.89647	3.20609	0.00000
H	-8.40185	-3.53400	0.88771
H	-8.40185	3.53400	-0.88771
H	-8.40185	3.53400	0.88771
H	-8.40185	-3.53400	-0.88771
C	4.86554	0.70679	0.00000
C	4.86554	-0.70679	0.00000
C	6.33026	-0.74780	0.00000
C	6.33026	0.74780	0.00000
O	7.17735	1.62710	0.00000
O	7.17735	-1.62710	0.00000
N	3.92182	1.63602	0.00000
N	3.92182	-1.63602	0.00000
H	2.93238	1.38594	0.00000
H	2.93238	-1.38594	0.00000
C	4.22133	-3.05874	0.00000
C	4.22133	3.05874	0.00000
H	5.30126	-3.20275	0.00000
H	5.30126	3.20275	0.00000

Chapter 3

H	3.79634	-3.53389	0.88753
H	3.79634	3.53389	-0.88753
H	3.79634	3.53389	0.88753
H	3.79634	-3.53389	-0.88753
C	11.02811	0.70047	0.00000
C	11.02811	-0.70047	0.00000
C	12.50110	-0.75901	0.00000
C	12.50110	0.75901	0.00000
O	13.32512	1.64846	0.00000
O	13.32512	-1.64846	0.00000
N	10.07464	1.63249	0.00000
N	10.07464	-1.63249	0.00000
H	9.09026	1.37673	0.00000
H	9.09026	-1.37673	0.00000
C	10.37044	-3.05366	0.00000
C	10.37044	3.05366	0.00000
H	11.45078	-3.19680	0.00000
H	11.45078	3.19680	0.00000
H	9.94769	-3.53326	0.88749
H	9.94769	3.53326	-0.88749
H	9.94769	3.53326	0.88749
H	9.94769	-3.53326	-0.88749

Total electronic energy = -2960.1976596 a.u.

ZPE = 0.858612 a.u.

NIm = 1 (6.63 i cm⁻¹)

1' "stacked" hexamer (C_s)

	X	Y	Z
C	9.70850	0.69718	0.26029
C	9.70850	-0.69718	0.26029
C	9.53235	0.76232	-1.20170
C	9.53235	-0.76232	-1.20170
N	9.78361	1.61684	1.22926
N	9.78361	-1.61684	1.22926
C	9.51627	3.02829	0.99213
C	9.51627	-3.02829	0.99213

O	9.37440	1.64780	-2.01036
O	9.37440	-1.64780	-2.01036
H	9.67787	-1.30193	2.18132
H	9.67787	1.30193	2.18132
H	8.50185	3.28306	1.31131
H	8.50185	-3.28306	1.31131
H	9.62572	3.23229	-0.07230
H	9.62572	-3.23229	-0.07230
H	10.23378	3.63803	1.54399
H	10.23378	-3.63803	1.54399
C	6.38080	-0.69982	-0.14557
C	-6.42173	-0.69718	-0.13587
C	6.38080	0.69982	-0.14557
C	-6.42173	0.69718	-0.13587
C	6.53097	-0.75901	1.31460
C	-6.24555	-0.76232	1.32612
C	6.53097	0.75901	1.31460
C	-6.24555	0.76232	1.32612
N	6.24919	-1.60541	-1.11002
N	-6.49684	-1.61684	-1.10483
N	6.24919	1.60541	-1.11002
N	-6.49684	1.61684	-1.10483
C	6.39968	-3.03463	-0.90035
C	-6.22952	-3.02829	-0.86770
C	6.39968	3.03463	-0.90035
C	-6.22952	3.02829	-0.86770
O	6.61597	-1.64573	2.14045
O	-6.08758	-1.64780	2.13478
O	6.61597	1.64573	2.14045
O	-6.08758	1.64780	2.13478
H	6.23455	1.29059	-2.06761
H	-6.39115	1.30193	-2.05689
H	6.23455	-1.29059	-2.06761
H	-6.39115	-1.30193	-2.05689
H	5.59552	-3.56465	-1.41403
H	-5.21511	-3.28307	-1.18689

Chapter 3

H	5.59552	3.56465	-1.41403
H	-5.21511	3.28307	-1.18689
H	6.33824	-3.23992	0.16782
H	-6.33897	-3.23229	0.19673
H	6.33824	3.23992	0.16782
H	-6.33897	3.23229	0.19673
H	7.36677	-3.37361	-1.28172
H	-6.94704	-3.63803	-1.41957
H	7.36677	3.37361	-1.28172
H	-6.94704	3.63803	-1.41957
C	3.25957	0.69855	0.12005
C	-3.09401	0.69982	0.27000
C	3.25957	-0.69855	0.12005
C	-3.09401	-0.69982	0.27000
C	3.09527	0.76088	-1.33914
C	-3.24419	0.75901	-1.19017
C	3.09527	-0.76088	-1.33914
C	-3.24419	-0.75901	-1.19017
N	3.38064	1.60469	1.08702
N	-2.96237	1.60541	1.23444
N	3.38064	-1.60469	1.08702
N	-2.96237	-1.60541	1.23444
C	3.25928	3.03589	0.87582
C	-3.11289	3.03463	1.02477
C	3.25928	-3.03589	0.87582
C	-3.11289	-3.03463	1.02477
O	2.99856	1.65032	-2.15851
O	-3.32920	1.64573	-2.01602
O	2.99856	-1.65032	-2.15851
O	-3.32920	-1.64573	-2.01602
H	3.42952	-1.29087	2.04365
H	-2.94778	-1.29059	2.19203
H	3.42952	1.29087	2.04365
H	-2.94778	1.29059	2.19203
H	2.32798	3.40506	1.31388
H	-2.30875	3.56466	1.53846

H	2.32798	-3.40506	1.31388
H	-2.30875	-3.56466	1.53846
H	3.25963	3.23298	-0.19577
H	-3.05144	3.23992	-0.04339
H	3.25963	-3.23298	-0.19577
H	-3.05144	-3.23992	-0.04339
H	4.10604	3.54916	1.33615
H	-4.07998	3.37360	1.40612
H	4.10604	-3.54916	1.33615
H	-4.07998	-3.37360	1.40612
C	0.02722	-0.69855	0.00435
C	0.02722	0.69855	0.00435
C	0.19154	-0.76088	1.46353
C	0.19154	0.76088	1.46353
N	-0.09385	-1.60469	-0.96263
N	-0.09385	1.60469	-0.96263
C	0.02752	-3.03589	-0.75142
C	0.02752	3.03589	-0.75142
O	0.28827	-1.65032	2.28291
O	0.28827	1.65032	2.28291
H	-0.81923	-3.54916	-1.21177
H	0.95883	-3.40505	-1.18949
H	-0.81923	3.54916	-1.21177
H	0.95883	3.40505	-1.18949
H	0.02718	-3.23298	0.32016
H	0.02718	3.23298	0.32016
H	-0.14276	1.29087	-1.91925
H	-0.14276	-1.29087	-1.91925

Total electronic energy = -2960.1844542 a.u.

ZPE = 0.859890 a.u.

NIm = 7 (32.95*i* cm⁻¹, 31.18*i* cm⁻¹, 28.55*i* cm⁻¹, 22.79*i* cm⁻¹, 21.35*i* cm⁻¹, 20.04*i* cm⁻¹, 17.92*i* cm⁻¹)

2' monomer (C_{2v})

	X	Y	Z
C	-0.04232	-1.40693	0.00000

Chapter 3

C	0.00000	0.00000	0.00000
C	1.40770	-1.49423	0.00000
C	1.45265	0.00000	0.00000
N	-1.04412	-2.28918	0.00000
N	-0.94697	0.94087	0.00000
C	-0.87735	-3.73616	0.00000
C	-0.69353	2.37521	0.00000
S	2.53441	-2.67520	0.00000
S	2.64829	1.11112	0.00000
H	-1.33456	-4.17163	0.89148
H	-1.33456	-4.17163	-0.89148
H	-1.12375	2.83737	0.89148
H	-1.12375	2.83737	-0.89148
H	0.18758	-3.96475	0.00000
H	0.38321	2.53938	0.00000
H	-1.90884	0.64332	0.00000
H	-1.98638	-1.93436	0.00000

Total electronic energy = -1139.267555 a.u.

ZPE = 0.136849 a.u.

NIm = 1 (12.92i cm⁻¹)

2' "head-to-tail" hexamer (C_{2v})

	X	Y	Z
C	0.66300	0.73442	0.00000
C	0.66300	-0.73442	0.00000
S	1.82073	1.91247	0.00000
S	1.82073	-1.91247	0.00000
C	-0.78430	0.71449	0.00000
C	-0.78430	-0.71449	0.00000
N	-1.75333	1.60101	0.00000
N	-1.75333	-1.60101	0.00000
H	-2.72309	1.28094	0.00000
H	-2.72309	-1.28094	0.00000
C	-1.56687	3.04519	0.00000
C	-1.56687	-3.04519	0.00000
H	-0.50250	3.27356	0.00000

H	-0.50250	-3.27356	0.00000
H	-2.03238	3.47521	-0.88911
H	-2.03238	-3.47521	0.88911
H	-2.03238	-3.47521	-0.88911
H	-2.03238	3.47521	0.88911
N	-15.47992	-1.60213	0.00000
N	-15.47992	1.60213	0.00000
C	-14.50982	-0.71330	0.00000
C	-14.50982	0.71330	0.00000
C	-13.06267	-0.73566	0.00000
C	-13.06267	0.73566	0.00000
S	-11.90712	-1.91232	0.00000
S	-11.90712	1.91232	0.00000
C	-15.29343	-3.04697	0.00000
C	-15.29343	3.04697	0.00000
N	-8.61219	-1.60143	0.00000
N	-8.61219	1.60143	0.00000
C	-7.64342	-0.71451	0.00000
C	-7.64342	0.71451	0.00000
C	-6.19622	-0.73432	0.00000
C	-6.19622	0.73432	0.00000
S	-5.03908	-1.91274	0.00000
S	-5.03908	1.91274	0.00000
C	-8.42584	-3.04591	0.00000
C	-8.42584	3.04591	0.00000
C	-21.42288	0.70968	0.00000
C	-21.42288	-0.70968	0.00000
C	-19.97467	-0.74009	0.00000
C	-19.97467	0.74009	0.00000
S	-18.82087	1.90649	0.00000
S	-18.82087	-1.90649	0.00000
N	-22.38984	1.61593	0.00000
N	-22.38984	-1.61593	0.00000
H	-23.34326	1.28894	0.00000
H	-23.34326	-1.28894	0.00000
C	-22.19070	-3.06224	0.00000

Chapter 3

C	-22.19070	3.06224	0.00000
H	-21.12283	-3.27202	0.00000
H	-21.12283	3.27202	0.00000
H	-22.64226	-3.50081	0.89154
H	-22.64226	3.50081	-0.89154
H	-22.64226	3.50081	0.89154
H	-22.64226	-3.50081	-0.89154
H	-16.44482	1.27732	0.00000
H	-16.44482	-1.27732	0.00000
H	-14.22877	-3.27373	0.00000
H	-14.22877	3.27373	0.00000
H	-15.75577	-3.47859	0.88995
H	-15.75577	3.47859	-0.88995
H	-15.75577	3.47859	0.88995
H	-15.75577	-3.47859	-0.88995
H	-9.58112	1.28060	0.00000
H	-9.58112	-1.28060	0.00000
H	-7.36152	-3.27425	0.00000
H	-7.36152	3.27425	0.00000
H	-8.89084	-3.47595	0.88930
H	-8.89084	3.47595	-0.88930
H	-8.89084	3.47595	0.88930
H	-8.89084	-3.47595	-0.88930
C	6.08825	0.71323	0.00000
C	6.08825	-0.71323	0.00000
C	7.53586	-0.73606	0.00000
C	7.53586	0.73606	0.00000
S	8.69415	1.91091	0.00000
S	8.69415	-1.91091	0.00000
N	5.11728	1.60068	0.00000
N	5.11728	-1.60068	0.00000
H	4.14865	1.27985	0.00000
H	4.14865	-1.27985	0.00000
C	5.30494	-3.04410	0.00000
C	5.30494	3.04410	0.00000
H	6.36988	-3.27059	0.00000

H	6.36988	3.27059	0.00000
H	4.84060	-3.47590	0.88911
H	4.84060	3.47590	-0.88911
H	4.84060	3.47590	0.88911
H	4.84060	-3.47590	-0.88911
C	13.02007	0.70865	0.00000
C	13.02007	-0.70865	0.00000
C	14.46978	-0.74262	0.00000
C	14.46978	0.74262	0.00000
S	15.63563	1.90051	0.00000
S	15.63563	-1.90051	0.00000
N	12.04132	1.59932	0.00000
N	12.04132	-1.59932	0.00000
H	11.07730	1.27481	0.00000
H	11.07730	-1.27481	0.00000
C	12.23284	-3.04013	0.00000
C	12.23284	3.04013	0.00000
H	13.30004	-3.25891	0.00000
H	13.30004	3.25891	0.00000
H	11.77319	-3.47879	0.88917
H	11.77319	3.47879	-0.88917
H	11.77319	3.47879	0.88917
H	11.77319	-3.47879	-0.88917

Total electronic energy = -6835.7542175 a.u.

ZPE = 0.831786 a.u.

NIm = 7 (19.29 icm^{-1} , 17.05 icm^{-1} , 14.19 icm^{-1} , 10.98 icm^{-1} , 7.87 icm^{-1} , 2.09 icm^{-1} , 1.33 icm^{-1})

2' "stacked" hexamer (C_s)

	X	Y	Z
C	9.70112	0.70895	0.11128
C	9.70112	-0.70895	0.11128
C	9.72480	0.74293	-1.33885
C	9.72480	-0.74293	-1.33885
N	9.66146	1.60739	1.08405
N	9.66146	-1.60739	1.08405

Chapter 3

C	9.64445	3.05070	0.89082
C	9.64445	-3.05070	0.89082
S	9.69034	1.88980	-2.51254
S	9.69034	-1.88980	-2.51254
H	9.49358	-1.27932	2.02396
H	9.49358	1.27932	2.02396
H	8.71412	3.46087	1.29034
H	8.71412	-3.46087	1.29034
H	9.71891	3.26464	-0.17435
H	9.71891	-3.26464	-0.17435
H	10.49204	3.50474	1.40805
H	10.49204	-3.50474	1.40805
C	6.47513	-0.71450	0.01264
C	-6.41433	-0.70895	0.01307
C	6.47513	0.71450	0.01264
C	-6.41433	0.70895	0.01307
C	6.46287	-0.73677	1.46176
C	-6.43806	-0.74293	1.46321
C	6.46287	0.73677	1.46176
C	-6.43806	0.74293	1.46321
N	6.48137	-1.60208	-0.95525
N	-6.37464	-1.60739	-0.95969
N	6.48137	1.60208	-0.95525
N	-6.37464	1.60739	-0.95969
C	6.46660	-3.04724	-0.78264
C	-6.35766	-3.05070	-0.76647
C	6.46660	3.04724	-0.78264
C	-6.35766	3.05070	-0.76647
S	6.45734	-1.88628	2.64870
S	-6.40363	-1.88980	2.63689
S	6.45734	1.88628	2.64870
S	-6.40363	1.88980	2.63689
H	6.50976	1.26863	-1.90899
H	-6.20669	1.27932	-1.89959
H	6.50976	-1.26863	-1.90899
H	-6.20669	-1.27932	-1.89959

H	5.57991	-3.45477	-1.27290
H	-5.42732	-3.46088	-1.16595
H	5.57991	3.45477	-1.27290
H	-5.42732	3.46088	-1.16595
H	6.44036	-3.27454	0.28178
H	-6.43217	-3.26464	0.29870
H	6.44036	3.27454	0.28178
H	-6.43217	3.26464	0.29870
H	7.36678	-3.47004	-1.23355
H	-7.20524	-3.50473	-1.28373
H	7.36678	3.47004	-1.23355
H	-7.20524	3.50473	-1.28373
C	3.25006	0.71323	0.10602
C	-3.18835	0.71450	0.11181
C	3.25006	-0.71323	0.10602
C	-3.18835	-0.71450	0.11181
C	3.25561	0.73837	-1.34315
C	-3.17607	0.73677	-1.33731
C	3.25561	-0.73837	-1.34315
C	-3.17607	-0.73677	-1.33731
N	3.24379	1.60308	1.07469
N	-3.19460	1.60208	1.07970
N	3.24379	-1.60308	1.07469
N	-3.19460	-1.60208	1.07970
C	3.24625	3.04769	0.89892
C	-3.17984	3.04723	0.90709
C	3.24625	-3.04769	0.89892
C	-3.17984	-3.04723	0.90709
S	3.25602	1.88845	-2.52560
S	-3.17052	1.88628	-2.52426
S	3.25602	-1.88845	-2.52560
S	-3.17052	-1.88628	-2.52426
H	3.23552	-1.27058	2.02888
H	-3.22300	-1.26863	2.03344
H	3.23552	1.27058	2.02888
H	-3.22300	1.26863	2.03344

Chapter 3

H	2.35196	3.46629	1.36559
H	-2.29315	3.45477	1.39736
H	2.35196	-3.46629	1.36559
H	-2.29315	-3.45477	1.39736
H	3.25048	3.27294	-0.16640
H	-3.15357	3.27454	-0.15734
H	3.25048	-3.27294	-0.16640
H	-3.15357	-3.27454	-0.15734
H	4.13821	3.46425	1.37184
H	-4.08002	3.47004	1.35798
H	4.13821	-3.46425	1.37184
H	-4.08002	-3.47004	1.35798
C	0.03672	-0.71323	0.01847
C	0.03672	0.71323	0.01847
C	0.03116	-0.73837	1.46764
C	0.03116	0.73837	1.46764
N	0.04299	-1.60308	-0.95020
N	0.04299	1.60308	-0.95020
C	0.04054	-3.04769	-0.77443
C	0.04054	3.04769	-0.77443
S	0.03074	-1.88846	2.65009
S	0.03074	1.88846	2.65009
H	-0.85142	-3.46426	-1.24735
H	0.93483	-3.46629	-1.24109
H	-0.85142	3.46426	-1.24735
H	0.93483	3.46629	-1.24109
H	0.03629	-3.27294	0.29089
H	0.03629	3.27294	0.29089
H	0.05127	1.27058	-1.90439
H	0.05127	-1.27058	-1.90439

Total electronic energy = -6835.8024592 a.u.

ZPE = 0.837358 a.u.

NIm = 3 (19.63 icm^{-1} , 15.84 icm^{-1} , 7.12 icm^{-1})

REFERENCES

- (1) Lamour, G.; Kirkegaard, J. B.; Li, H.; Knowles, T. P.; Gsponer, J. *Source Code Biol. Med.* **2014**, *9* (1), 16.
- (2) Saez Talens, V.; Englebienne, P.; Trinh, T. T.; Noteborn, W. E. M.; Voets, I. K.; Kieltyka, R. E. *Angew. Chemie - Int. Ed.* **2015**, *54* (36), 10502.

